Available online at www.sciencedirect.com
SCIENCE DIRECT®
Deep-Sea Research I 53 (2006) 627–655
DEEP-SEA RESEARCH PART I
www.elsevier.com/locate/dsr

Sub-inertial modulation of semi-diurnal currents over the continental slope in the Faeroe-Shetland Channel

Phil Hosegood*, Hans van Haren

Royal Netherlands Institute of Sea Research (NIOZ), P.O. Box 59, 1790 AB Den Burg, The Netherlands

Received 21 January 2005; received in revised form 15 December 2005; accepted 27 December 2005
Available online 23 March 2006

Abstract

Observations were made over the continental slope in the Faeroe-Shetland Channel with the purpose of studying motions in the semidiurnal tidal frequency band and their interaction with background conditions. Specifically, the study focused on internal (baroclinic) tidal motions associated with internal gravity waves. In the internal tide (IT) source region, kinetic energy spectra reveal a fall-off rate with frequency of σ^{-2} which is associated with the passage of strongly non-linear fronts at the sea-bed. At a distance of 10 km off shore from the source region spectra from both the permanent pycnocline and weakly stratified interior exhibit a fall-off rate of σ^{-3}, indicative of a regime in which internal waves are dominated by higher harmonics of the M_2 semidiurnal tidal frequency as a result of non-linear advection. The bandwidth, $\Delta\sigma = 0.23-0.3$ cycles per day (cpd) of the semidiurnal band determined from the distribution of baroclinic energy outside the deterministic tidal frequencies, implies a modulation period of 3.3–4.3 days and which is observed as pulses of semidiurnal energy that are not related to the spring–neap cycle. The period of modulation is related to changes in the background stratification and the low-frequency vorticity. Variations in stratification are sufficient to modify the IT path by >150 m in the vertical over a horizontal distance of 10 km.The cross-slope gradient of the low-frequency ($\sigma < 0.75$ cpd) long-slope velocity, $\partial V/\partial x$, which represents one component of the vorticity varies with a periodicity of 3–4 days and has a magnitude sufficient to increase the effective Coriolis frequency to a value larger than M_2 so that the IT is unable to propagate as a free internal gravity wave. The source of the subinertial variability in the background conditions is attributed to meteorologically forced continental shelf waves which respond in two ways to prevailing winds and which perturb the pre-existing geostrophic balance that exists over the slope; oscillatory, clockwise rotating currents with a frequency of $0.7 \times f$, where f is the Coriolis frequency, result from short impulsive winds whilst a quasi-steady long-slope flow persists as long as stronger winds of longer duration prevail. The impact of the observed subinertial variability in low-frequency vorticity and stratification raises doubts as to whether an 'attractor', along which internal wave energy is found following repeated reflections within a confined basin, may be observed in such a dynamic environment.

Keywords: Internal tide; Intermittency; Continental shelf waves; UK; Faeroe-Shetland Channel; 60° 30′N 2°W–61° 30′N 5°W

1. Introduction

The forcing of internal tides (IT) over continental shelves throughout the oceans is generally well understood. The interaction of barotropic tidal

*Corresponding author. Present address: Applied Physics Laboratory, University of Washington, 1013 NE 40th Street, Seattle, Washington, DC 98105, USA. Tel.: +1 206 897 1446; fax: +1 206 543 3521.
E-mail address: hosegood@apl.washington.edu (P. Hosegood).

0967-0637/$ - see front matter © 2006 Elsevier Ltd. All rights reserved.
doi:10.1016/j.dsr.2005.12.016

currents with sloping topography in the presence of density stratification generates baroclinic internal gravity waves of tidal frequency (e.g. Prinsenberg et al., 1974; Baines, 1982). Generation is thought to occur over the slope and principally near the largest stratification above the upper slope and at locations where the angle of inclination of the IT characteristic with respect to the horizontal, α:

$$\sin^2\alpha = \frac{\sigma^2 - f^2}{N^2 - f^2} \tag{1}$$

matches the bottom slope, γ, where σ is the frequency, $f = 2\Omega \sin\varphi$ is the Coriolis frequency, twice the local vertical component of the Earth's rotation vector Ω at latitude φ ($1.27 \times 10^{-4}\,s^{-2}$ at 61 °N), and N is the buoyancy frequency:

$$N(z) = \left(\frac{g}{\rho_0}\frac{\partial\rho}{\partial z}\right)^{1/2}, \tag{2}$$

where g is the acceleration due to gravity, ρ_o is a reference value of the density field and $\partial\rho/\partial z$ is the change in the density field over a suitable depth range. Assuming along-slope uniformity and introducing a stream function Ψ which expresses the baroclinic cross-slope and vertical current speeds as $u = \partial\psi/\partial z$ and $w = -\partial\psi/\partial x$, the linear hydrostatic equations governing IT generation are (Gerkema, 2001):

$$\frac{\partial^3\psi}{\partial z^2\partial t} - f\frac{\partial v}{\partial z} - \frac{\partial\rho}{\partial x} = 0, \tag{3}$$

$$\frac{\partial v}{\partial t} + f\frac{\partial\psi}{\partial z} = 0, \tag{4}$$

$$\frac{\partial\rho}{\partial t} + N^2\frac{\partial\psi}{\partial t} = -\frac{zN^2Q\sin\sigma t}{[H - h(x)]^2}\frac{\mathrm{d}h}{\mathrm{d}x}, \tag{5}$$

where in (3)–(5) ρ represents the perturbation density field, $\rho(x,y,z,t)$. The right-hand side of Eq. (5) represents the forcing of the IT by a barotropic flow over topography, where Q is the cross-slope barotropic flux. This forcing term indicates that IT generation tends to occur not just over critical slopes but also as an increasing function of bottom slope, $\mathrm{d}h/\mathrm{d}x$, and stratification, N^2.

For sufficiently steep topography, i.e. large $\mathrm{d}h/\mathrm{d}x$, and in the presence of continuous stratification beams of energy are predicted to emanate from the generation site and to propagate in both the shoreward and seaward directions along characteristics according to Eq. (1) (deWitt et al., 1986; Pingree and New, 1991; Lien and Gregg, 2001; Lam et al., 2004). Within the vicinity of the source region they may be coherent with the barotropic tide (cIT) (Schott, 1977).

Further from the source region friction and thermal diffusion act to preferentially dampen higher modes (Wunsch, 1975) such that observations of narrow beams aligned with the characteristics may be made only near the source region (Huthnance, 1989; Gerkema, 2001). Thereafter the lowest modes tend to dominate observations and may propagate away from the source region without significant dissipation until reaching a boundary (Ray and Mitchum, 1997; Cummins et al., 2001; Nash et al., 2004). Far from generation regions where they have had time to interact with background conditions and undergo reflection from boundaries, IT are considered to be intermittent and to have an unstable phase (Ekman, 1931; Wunsch, 1975). Such incoherent internal tides (icIT) may be observed at frequencies outside the deterministic tidal frequencies that force them (van Haren, 2004a) and require sufficiently long records to separate the icIT from the deterministic signal, albeit in the knowledge that the latter contains both the barotropic signal and the cIT. The situation is complicated further by recent evidence suggesting that low-mode internal waves which are in fact phase locked to the deterministic barotropic tide account for open ocean baroclinic energy amounting to ~25% of barotropic tidal energy (Dushaw et al., 1995; Ray and Cartwright, 2001). This implies that it is important to consider the structure of the motions in order to discriminate between barotropic and coherent baroclinic tidal motions (cIT) at deterministic tidal frequencies.

The source of IT intermittency is generally attributed to varying background conditions. In the Bay of Biscay large scale variations in the stratification result in a 5–7 days intermittency in the icIT which comprises 30% of the total tidal kinetic energy in the semidiurnal tidal band (van Haren, 2004a). The incoherent modulation of the IT in Mamala Bay, Hawaii, is also proposed to result from the remote generation and subsequent propagation of the IT into the Bay through variable stratification and mesoscale activity (Eich et al., 2004) as opposed to the generation and subsequent modulation of the IT within the bay itself by *local* variability in stratification. Large phase shifts may occur in the *baroclinic* spring–neap cycle (and thus in the spatial position of spring tides) due to the different ray paths taken by the different harmonic

constituents and which are intimately dependent on the temporal variability of the stratification (Gerkema, 2002). The results are relevant to observations made in an Eulerian frame of reference as the spatially confined baroclinic signal may simply be missed by an instrument fixed in space as a result of the change in ray path of the IT (van Haren, 2004a). One of the original aims of the current field study was to study internal wave focusing along 'attractors' following the repeated reflection of internal waves from sloping boundaries in a confined basin, a process whereby energy propagation is not just confined to IT characteristics. Internal wave focusing was demonstrated in laboratory experiments by Maas et al. (1997) in which N was constant across the basin. A variation in time across the basin in N or another background field such as subinertial vorticity (Mooers, 1975) will modulate the ray path however and cause a more complicated attractor pattern along which the internal wave energy is concentrated and which may therefore be more difficult to observe. In the case that the background fields vary on timescales shorter than those required for multiple reflections of the internal waves to occur, the attractors (which by definition require multiple reflections) may not be able to form. In particular, non-uniformities in stratification and shear (and thus vorticity) in the interior of the basin may prohibit the transmission of internal wave energy further into the basin, with catastrophic results for the formation of an attractor due to the lack of reflections from the basin sides.

In a broader context the interaction of internal tidal motions with the background fields has further implications for the cascade of energy from large to small scales within the internal wave band (IWB) constrained in the frequency range $f<\sigma<N$, $N \gg f$. For $f \ll \sigma \ll N$, the IWB is characterized by a spectral fall-off rate with frequency of σ^{-p}, where $-2.5<p<1.5$ according to the Garrett and Munk (1972) canonical spectrum. Recent evidence suggests that in regions 'far' away from the sources of tidal–inertial interactions the spectrum is properly represented by the GM spectrum. The fall-off rate of a smooth internal wave spectrum tends to σ^{-3} and is indicative of the non-linear advection dynamics that determine the nature of the spectrum outside the tidal and inertial peaks (van Haren, 2004b). Thus the rate of energy transfer to small scales where oceanic mixing occurs depends not only on the nature of the interaction between tidal and background conditions but also on the proximity of a particular location to where these interactions occur.

In this paper observations are presented from a variety of moorings sampling current and temperature variability located mid-way along the continental slope in the Faeroe-Shetland Channel (FSC) in an attempt to establish whether there is a baroclinic response to the barotropic tidal flow and if so, what form it takes. Previous observations in the FSC have revealed the near bed region to be subject to widespread turbulent mixing as a result of the asymmetric response of the bottom boundary layer (BBL) to the prevailing barotropic tidal flow (Hosegood and van Haren, 2003) which, common to many continental slopes, flows principally along the slope and is therefore not ideal for IT generation (Sjoberg and Stigebrandt, 1992). Internal bores have also been observed to propagate up the slope with an apparent sub-inertial frequency (Hosegood and van Haren, 2004), therefore appearing to preclude IT as the source of such features. Microstructure observations however suggest turbulence in the interior of the channel to be potentially the result of IT propagation from the Shetland slope (Hosegood et al., 2005). Applying Eqs. (3)–(5) to the bathymetry of the Faeroe-Shetland using measured cross-slope barotropic fluxes and a stratification profile from a central location in the channel but taken to be uniform in the cross-slope direction, generation is predicted by Gerkema (2002) to occur immediately over the Shetland slope from a depth of 450 m upwards to the shelf break, and also at a height above the bed of ~100 m within the permanent pycnocline at depths of 400–500 m (See Fig. 11, Hosegood et al., 2005). In reality the pycnocline deepens by >100 m over the Shetland slope with respect to the centre of the channel however (Fig. 3 in Hosegood et al., 2005), and the location of IT generation may thus be found at a depth of ~600 m and shallower. The deterministic signal is therefore studied first in both the IT source region and in an off-shore location to determine whether it is purely barotropic or whether it contains a coherent internal tide (cIT). Kinetic energy spectra are used to firstly identify the dominant motions in frequency space but also as an indication of the background field within which tidal motions act, and potentially with which they *interact*. Secondly we consider the residual currents in the semidiurnal frequency band (the icIT) following removal of the barotropic component as an indication of the intermittence of the baroclinic

signal and the role played by the background conditions. We then assess the apparent influence of the background conditions on our results given previous observations from the study region which suggest a subinertial modulation of the baroclinic currents over the slope.

2. Field study and methods

2.1. The Faeroe-Shetland Channel

The FSC is a semi-enclosed basin located to the north of Scotland (Fig. 1) and running in a predominantly north-east/south-west orientation such that the long-slope axis of the channel is defined at a heading of 52 °N. The seafloor is revealed by seismic studies to be smooth with no topographic irregularities such as ridges or canyons that could be expected to perturb the mean flow (STRATEGEM Partners, 2003). A contourite deposit at approximately 700 m depth on the Shetland slope causes a change in bottom slope, α, which decreases from 0.028 ± 0.0052 radians below 700 m depth to 0.0145 ± 0.0027 radians between 700 and 450 m depth. A permanent pycnocline is found at depths between 400 and 700 m, depending on the relative position in the channel. Over the Shetland slope in particular the depth of maximum stratification varies over a timescale of days, with typical maximum values of $N^2 \approx 2 \times 10^{-4}\,\mathrm{s}^{-2}$. The reader is referred to Turrell et al. (1999) for further details of the long-term, large-scale hydrography of the area.

Over the Shetland slope the boundary current represents an energetic poleward transport, with a warm, saline, buoyant core at a depth of typically 350 m in water of depth 400–1000 m (Turrell et al., 1999). Significant mesoscale variability occurs over the Shetland slope; the boundary current has been observed to be occasionally deflected into the central region of the channel (Sherwin et al., 1999), purportedly resulting from a large scale movement of water in the lower part of the water column beneath the permanent pycnocline. A 5–10 days periodicity observed in isotherm oscillations of amplitude ≈ 100 m is explained by Oey (1998) as flow instability in the slope current at the southern end of the channel and which then propagates northwards along the Shetland slope as a meander of the slope current. As the current and temperature variations extend below the mixed layer they are not directly forced by wind-stress, and have periods

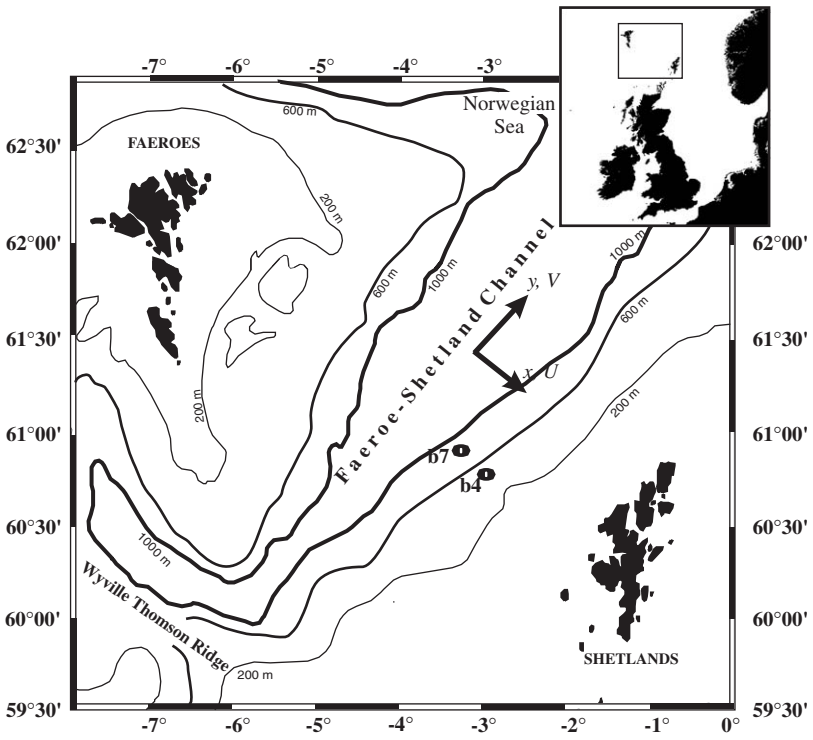

Fig. 1. Map of study region, indicating the position of the short-term ADCP moorings within the channel and the axes orientation.

much longer than IT, thus further discounting tidal forcing. Eddies are also a fairly common phenomenon over the Shetland slope, traveling at speeds of ca. 8 cm s^{-1} and with a period of 14 days (Smyth, 1995; Sherwin et al., 1999). Explanations for their generation include instability of the slope current (Huthnance, 1989), which may occur due to upwelling at the shelf break in response to northernly winds, causing horizontal shears which are then conducive for horizontal shear instability (Hackett and Røed, 1998).

2.2. Experimental set-up

Observations were made in the FSC during two cruises. Short-term moorings were deployed during PROCS-1 in the period 14th April–5th May 1999 (Yearday, $t = 103-124$) and PROCS-3 from 21st September–13th October 1999 ($t = 263-285$). Moorings were also deployed during the 4-month periods between the cruises, PROCS-2 ($t = 120-265$) and is referred to as the long-term moorings. Moorings were situated along a transect perpendicular to the Shetland slope, approximately half way along the channel, between depths of 471 and 1000 m (Fig. 2). Table 1 summarises the positions and sampling characteristics of each instrument. Here we focus on the current observations using 75 kHz RDI long-ranger acoustic Doppler current profilers (ADCP). The limited range (of ~300 m) of the ADCPs prohibited the determination of the barotropic current as the depth-averaged flow but their broadband operation ensured a low standard deviation of the measured currents.

Previous observations indicate the strong stratification of the permanent pycnocline potentially brings the slope between depths of 500 and 700 m to criticality for the M_2 IT (van Raaphorst et al., 2001; Hosegood and van Haren, 2004), in accordance with the model of Gerkema (2002). This is therefore considered as the potential source region for any IT generated over the Shetland slope (indicated by circles in Fig. 2). The ADCPs at moorings 1b4 and 3b4 are thus located in the source region but the lower ADCPs (at 1b7, 2b7, 3b7) are moored beneath the pycnocline at an offshore distance of 10 km from the source region (moorings 1b4, 3b4). A NIOZ thermistor string (van Haren et al., 2001) was deployed at 495 m depth during PROCS-1 (mooring 1a2) and sampled between heights (measured vertically) above the bed, z, of 2–34 m. This

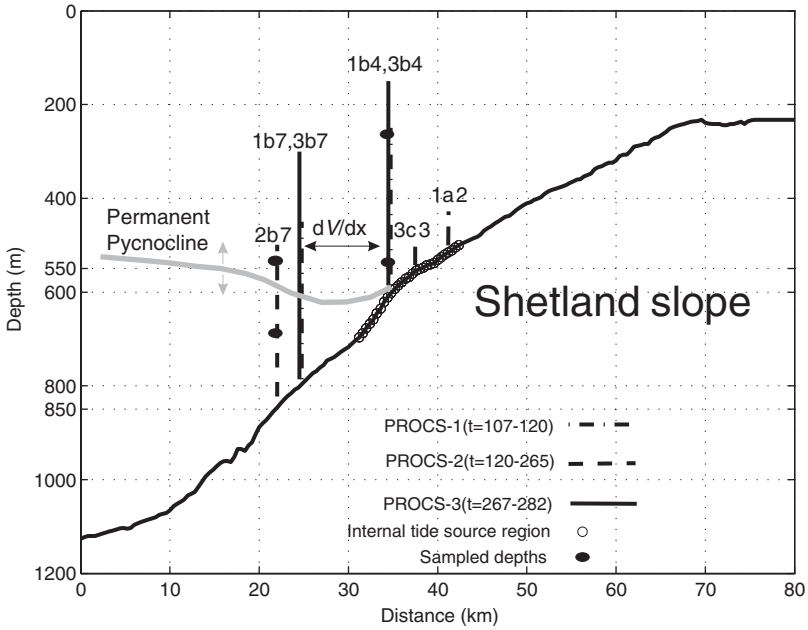

Fig. 2. Schematic cross-section of mooring locations over the Shetland slope and the approximate position of the permanent pycnocline. The cross-slope gradient of long-slope velocity, $\partial V/\partial x$ is calculated between moorings b4 and b7 during the short-term deployments. The potential source region for the internal tide, indicated by the circles at the seabed, is approximated as the part of the slope where CTD observations indicate sufficiently strong stratification to generate critical conditions according to Eq. (1). The depths chosen for analysis at each mooring are indicated by solid black ellipses.

Table 1
Summary of instrument deployment during PROCS

Mooring and position	Instrument	Depth (m)	Deployment period (Yearday)	Sampling depth range (m)	Sampling interval (min)
1b4 60°53′N, 3°06′W	LR-ADCP	600	107–120	586–250	5
1b7 60°58′N, 3°14′W	LR-ADCP	600	107–120	786–450	5
1a2 60°49′N, 2°59′W	NIOZ thermistor string	495	107–120	445–493	0.5
2b7 60°58′N, 3°15′W	LR-ADCP	850	120–265	823–499	10
3b4 60°54′N, 3°02′W	LR-ADCP	800	267–282	586–150	5
3b7 60°59′N, 3°10′W	LR-ADCP	800	267–282	786–300	5
3c3 60°57′N, 3°07′W	RCM-8	550	267–282	503, 516 529, 542	1

All long-ranger acoustic Doppler current profilers (LR-ADCP) had a vertical sampling resolution, $z = 4$ m and a range dependent on the number of acoustic scatterers in the water column and which is thus variable over time, typically by ± 50 m. The deployment period of each mooring is indicated by the prefix, 1, 2 and 3 for PROCS-1, PROCS-2 and PROCS-3, respectively. RCM-8 are mechanical current meters.

mooring only periodically samples the permanent pycnocline as it passes up the slope, whilst during PROCS-3 the mooring deployed at 550 m depth (3c3) sampled currents and temperature with mechanical Aanderaa recording current meters (RCM-8 s) at a sampling interval of 1 min where it is almost permanently within the pycnocline.

For the initial purposes of assessing the tidal motions we focus on the results from the ADCP in the long-term mooring, 2b7, due to its significantly longer time-series (~140 days as opposed to ~12 days for the short-term moorings) which resolves the various tidal constituents. We also consider data from the shallower short-term ADCPs, 1b4 and 3b4, as an indication of conditions in the source region. Later the short-term ADCPs at 800 m depth, 1b7 and 3b7, and the temperature data from the two cruises are used in assessing the subinertial variability of the background conditions.

2.3. Data handling

Spectral analysis is performed using Welch's averaged periodogram method on the time series from selected depth intervals. Varying degrees of freedom, ν, are used depending on the spectral resolution required. The longer time series provided by 2b7 allows $\nu = 36$ whilst resolving to a sufficient degree the spectral features of interest throughout the entire kinetic energy spectrum, but for the purpose of resolving the individual tidal constituents in the semi-diurnal band we use $\nu = 10$. For 1b4 and 3b4 the shorter time-series requires $\nu = 8$ for sufficient resolution at the expense of high accuracy. Depths corresponding to the permanent pycnocline and the weakly stratified interior are selected for detailed analysis (indicated in Fig. 2 as black ellipses). At 2b7 the depth appropriate to the interior and outside the influence of the BBL is determined from depth-profiles of kinetic energy at the dominant semidiurnal tidal constituents (Fig. 3). Kinetic energy begins to decay towards the bed at a depth of 700 m at all three principal tidal frequencies but not at the local inertial frequency, f, which is more than a decade less energetic than the weakest tidal constituent, N_2. CTD casts indicate a sharp decrease to $N^2 < 10^{-6}\,\mathrm{s}^{-2}$ below 700–750 m depth (throughout the paper $\Delta z = 20$ m when calculating N^2). A BBL of 150 m thickness is large but previous work has revealed the growth of the BBL over the slope to a commensurate thickness due to its asymmetric response to a long-slope flow (Hosegood and van Haren, 2003). We thus take the depths of 527 m ($N^2 > 10^{-5}\,\mathrm{s}^{-2}$) and 700 m ($10^{-6}\,\mathrm{s}^{-2} > N^2 > 10^{-5}\,\mathrm{s}^{-2}$) as indicative of the permanent pycnocline and weakly stratified interior, respectively, at 2b7. At the shallower, short-term moorings, 1b4 and 3b4, in water of depth 600 m the depths of 265 and 550 m are taken as the interior and permanent pycnocline, respectively. Here the pycnocline is close to the bottom but the strong stratification reduces the height, h, of the BBL according to $h = \sqrt{2}v_i/\gamma N$ where γ is a measure of the bottom slope and v_i is the interior flow (see Hosegood and van Haren, 2003). For $N \approx 50$ cycles per day (cpd) which is typical of the permanent

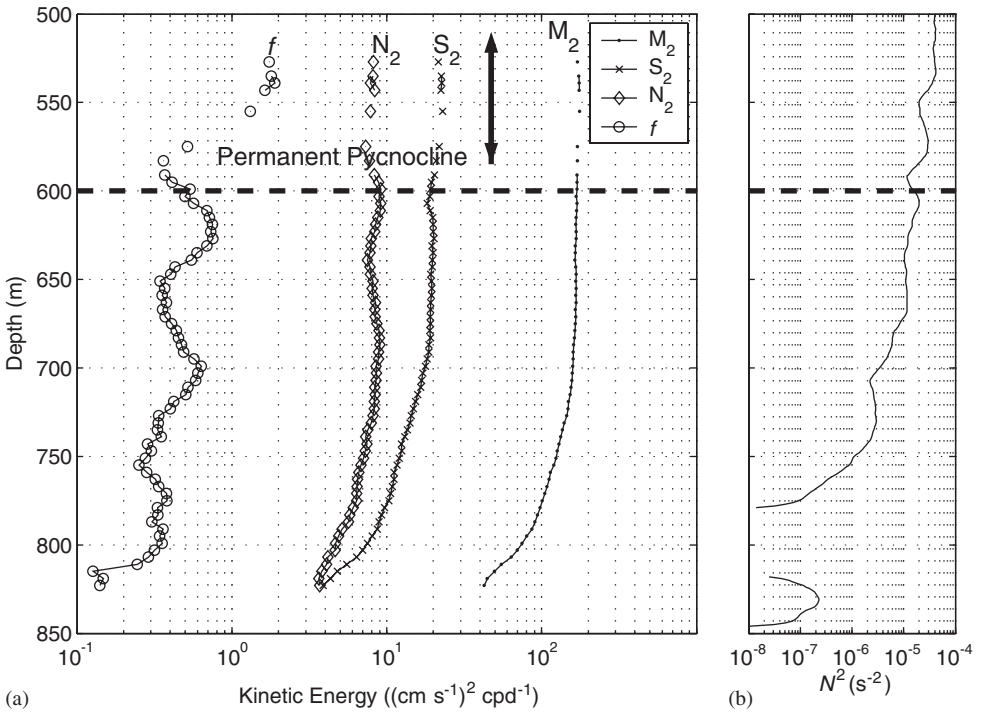

Fig. 3. (a) Kinetic energy depth profiles of the M_2, S_2, N_2 tidal constituents and the inertial frequency, f, from mooring 2b7 in 850 m water depth and (b) a typical N^2 profile from a nearby site. The (approximate) lower edge of the permanent pycnocline is indicated by the dashed line at a depth of 600 m.

pycnocline, $h<50$ m and the depth analysed here is thus outside the BBL.

Rotary spectra (Gonella, 1972) may be used to distinguish between barotropic and coherent baroclinic motions, freely propagating internal waves, non-linearly forced motions and fine structure contamination (van Haren, 2003), with freely propagating internal gravity waves having a current ellipticity $\varepsilon\sim|f/\sigma|$. Rotary amplitude spectra are defined as

Anti-clockwise spectrum:

$$P_+(\sigma)=\langle w_+\rangle^*\langle w_+\rangle/2, \tag{6a}$$

clockwise spectrum:

$$P_-(\sigma)=\langle w_-\rangle^*\langle w_-\rangle/2, \tag{6b}$$

where the angle brackets denote the Fourier transform and w_+, w_- are anticlockwise and clockwise rotary components, respectively. The measure of polarisation is given by the difference between rotary spectra and is defined as the rotary coefficient (Gonella, 1972):

$$C_R(\sigma)\equiv(P_-(\sigma)-P_+(\sigma))/P_{KE}(\sigma), \tag{7}$$

where $C_R=0$ for purely rectilinear motion and ±1 for purely circular motion and $P_{KE}=P_-+P_+$. The sign indicates the direction (clockwise or anticlockwise) in which the ellipse is traversed. Assuming linear perturbation and neglecting frictional stresses, the free internal wave solution to (7) becomes

$$|C_R(\sigma)|=\frac{|W_-^2-W_+^2|}{|W_-^2+W_+^2|}=\frac{2\sigma f}{\sigma^2+f^2},\quad \text{when } |\pi_+|=|\pi_-|, \tag{8}$$

where $W_{-,+}$ is the amplitude of the clockwise, anticlockwise rotary components, respectively, with equal forcing in the each component, i.e. symmetric forcing in one Cartesian direction only: e.g. $\pi_x=0$ or $\pi_y=0$ where π is the pressure gradient. Within the internal wave band (8) describes free gravity waves. As $\sigma\to N$, the near-rectilinear motions can be considered as circular motions in a plane tilted progressively towards the vertical for increasing σ (van Haren, 2003). In Section 3, we use C_R spectra to identify internal wave polarisation and thus differentiate between free internal waves and other motions within the internal wave band. As a

reviewer pointed out however, it should be noted that circumstances exist when Eq. (8) is not a good diagnostic for freely propagating waves, for example near a vertical wall where the superposition of an incident and reflected wave requires rectilinear motion.

Harmonic analysis (Dronkers, 1964) is performed on the time-series from moorings 1b4, 3b4 and 2b7 at 20 m vertical intervals (i.e. every 5th bin). Output is in terms of current ellipse parameters; semi-major and semi-minor axes amplitudes, orientation (relative to the direction of isobaths), and phase computed relative to GMT. The resulting tidal prediction, u_0,v_0 which is considered as the deterministic signal, is defined as the sum of those tidal constituents with a signal-to-noise ratio, SNR > 2:

$$u_o = \sum_n U_n \cos(\varphi_n + \sigma_n t), \tag{9}$$

where U_n is the amplitude of the nth constituent, φ_n is its phase and σ_n is the frequency at time t. It should be noted that only the length of the time series obtained from 2b7 resolves the M_2, N_2 and S_2 semi-diurnal tidal constituents and as such we focus on this mooring when addressing the baroclinic currents due to its ability relative to the short-term moorings to accurately identify and extract these deterministic signals.

3. Observations

3.1. Deterministic signal

3.1.1. Kinetic energy spectra

At mooring 2b7 kinetic energy (KE) in the permanent pycnocline (PP) at 527 m depth (blue line, Fig. 4(a)) and in the interior at 700 m depth (red line, Fig. 4(a)) are the same to within a factor of 2 of each other at sub-tidal frequencies, $\sigma < D_2$ (D_2 refers to the semi-diurnal band which includes the principal tidal constituents and M_4-f, D_1 refers to

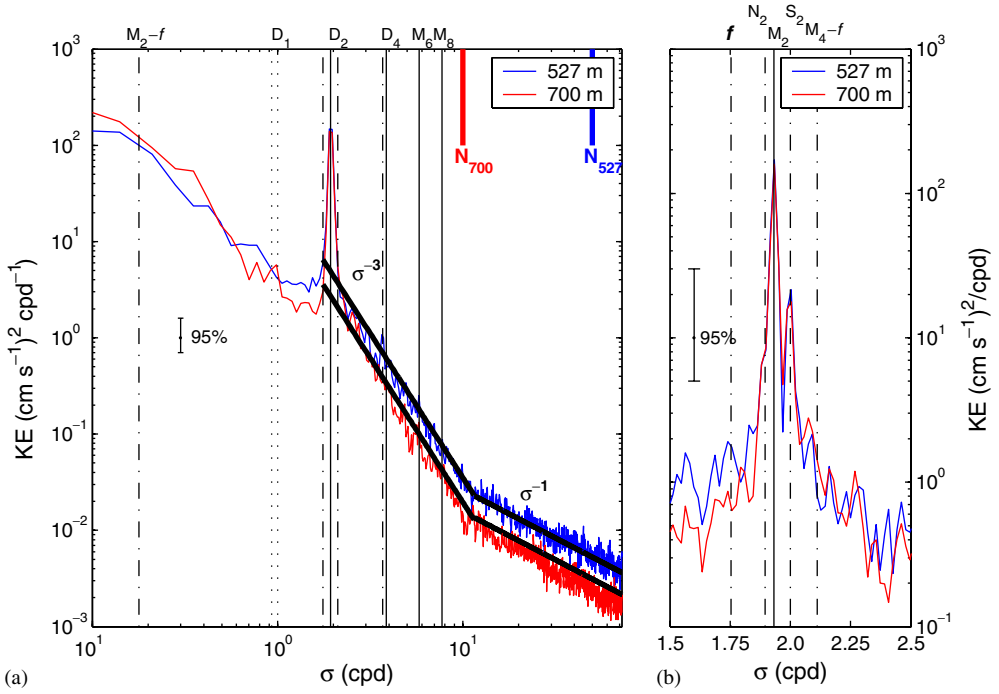

Fig. 4. (a) Moderately smoothed ($\nu = 30$ degrees of freedom) kinetic energy spectra from depths of 527 m (blue) and 700 m (red) at mooring 2b7, deployed for 140 days in water of depth 850 m and (b) nearly raw spectra ($\nu = 8$) for the same time series in the frequency range $1.5 < \sigma < 2.5$ cycles per day. The two depths correspond to the permanent pycnocline and the weakly stratified interior, respectively, and the corresponding buoyancy frequencies calculated from CTD casts at the mooring sites are indicated along the top x-axis of (a). Vertical black lines represent the M_2 tidal frequency and higher harmonics thereof, dash–dot lines to f and inertial-tidal interaction frequencies (e.g. M_2+f) and dotted lines to the diurnal tidal constituents, O_1 and K_1; in (a) the labels D_1, D_2 and D_4 refer to the diurnal, semi-diurnal and quarter-diurnal frequency bands. The sloping solid black lines in (a) represent the fall-off rates of energy with frequency for $\sigma > f$, and are labeled accordingly.

the diurnal frequency band and D_4 to the quarter-diurnal which incorporates the higher harmonics of the principal semi-diurnal tides like M_4, MS_4 and S_4, and interaction frequencies such as M_2+f, etc.). At $=D_2$, KE is the same at both depths whilst there is no significant peak at $f=1.754$ cpd. For $\sigma>\mathrm{D}_2$, KE in the PP is consistently higher than in the interior by approximately a factor of 2–4 at all frequencies as indicated by the offset in σ^{-3} energy fall-off rates at both depths (indicated by sloping solid black lines in Fig. 4(a)) until $\sigma\approx 10$ cpd at which point the fall-off rate changes abruptly to σ^{-1} at both depths. The transition frequency, $\sigma_t\approx 10$ cpd is the same at both depths despite a significantly different width of the IWB because of the respective values of $N_{700}\approx 10$ cpd and $N_{527}\approx 50$ cpd (indicated on the top x-axis of Fig. 4(a) and calculated from CTD casts).

Within the IWB there is limited evidence of energy enhancement extending above the background continuum at higher tidal harmonic and tidal–inertial interaction frequencies, with the degree of enhancement varying depending on the depth. The greater spectral resolution afforded by a reduction in statistical reliability enables the separation of the D_2 band into its tidal (and inertial) constituents (Fig. 4(b)). M_2 is dominant whilst S_2 is a decade less energetic. N_2 is largely incorporated into the shoulders of M_2 with the smoothing employed here and f is largely insignificant in comparison to the tidal frequencies.

The results from mooring 1b4 (Fig. 5(a)) and 3b4 (Fig. 5(b)) in 600 m water depth are indicative of the expected source region for the IT. The significant difference between the moorings at 600 m as compared to 850 m depth is the fall-off rate (indicated by the sloping black line and which is the same for both 1b4 and 3b4 in Fig. 5 for comparative purposes) in the IWB which is σ^{-2} at $\sigma<\sigma_t$, extending uninterrupted to subinertial frequencies with the exception of the D_2 peak. At 550 m depth KE is enhanced by a factor of 2–5 at all

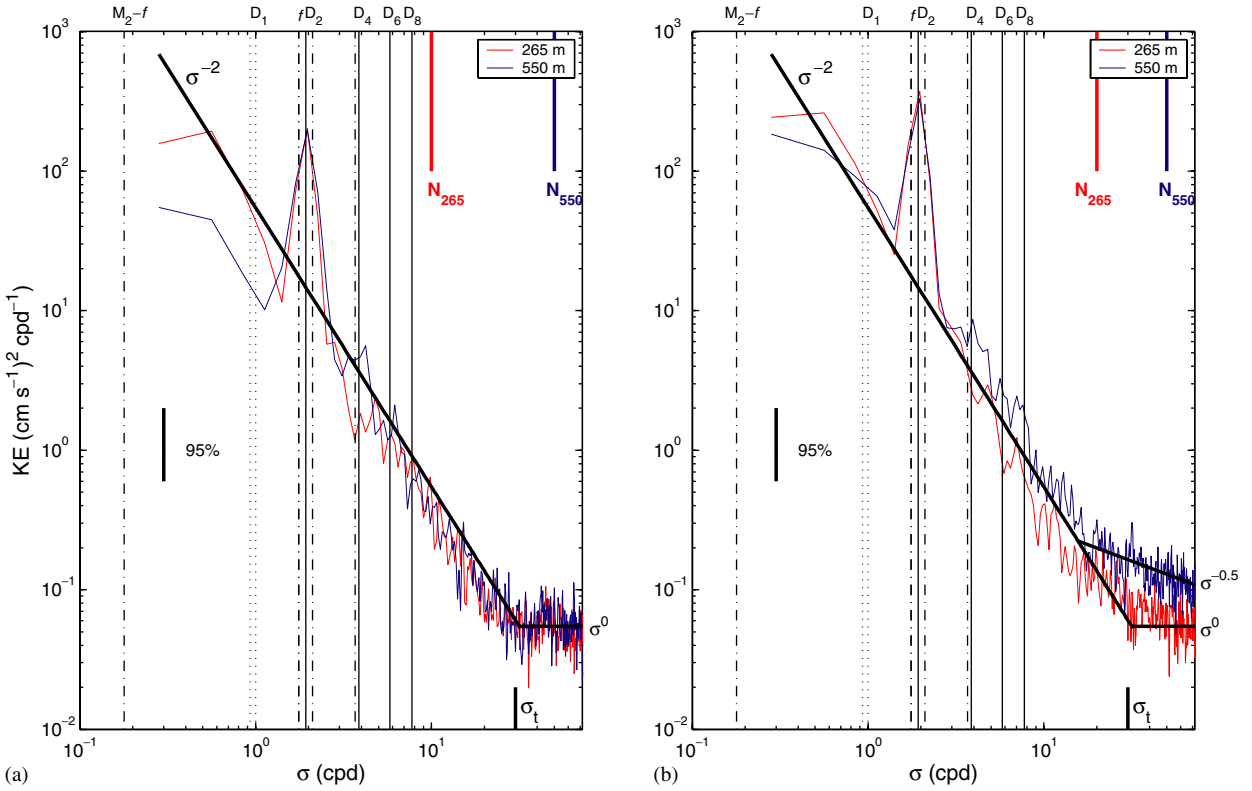

Fig. 5. As for Fig. 4(a) for short-term moorings (a) 1b4 and (b) 3b4 in water of depth 605 m and with $\nu=8$. Two depths are shown, 265 m (red line) and 550 m (blue line) corresponding to the weakly stratified interior and the permanent pycnocline, respectively. The transition frequency at which the fall-off rate changes, σ_t, is indicated on the bottom x-axis of each plot. The sloping black lines indicating the fall-off rate are identical for both deployment periods except the addition of $\sigma^{-0.5}$ in (b) at $\sigma>\sigma_t$.

frequencies in September-October (mooring 3b4, Fig. 5(b)) relative to the cruise in April–May (mooring 1b4, blue line, Fig. 5(a)). The transition frequency, $\sigma_t \approx 25$ cpd, at which the spectral slope changes is a factor of 2 larger than the deeper long-term mooring, 2b7. At 1b4 the spectral slope changes abruptly from σ^{-2} to σ^{-0} (i.e. white noise), with equal KE observed at both depths. Five months later (i.e. mooring 3b4) the spectral slope tends to a fall-off rate of $\sigma^{-0.5}$ at $\sigma > \sigma_t$ and with KE at 550 m (where N may often be >100 cpd) a factor of 4–5 larger than at 265 m depth where the weak stratification supports a narrower IWB. The transition is also less abrupt. In both cruises a broad enhancement of KE is observed in the near-bed region throughout D_4 and, during the second cruise, at M_6 and M_8 in the permanent pycnocline at 550 m.

3.1.2. Rotary spectra

The spectral fall-off rate differs between the moorings in 850 and 600 m of water, suggesting the prevalence of different mechanisms governing the distribution of energy throughout the IWB. However, results show that at neither location do currents exhibit polarisations indicative of freely propagating internal waves, with motions predominantly rectilinear as evidenced by low C_R. At 2b7 there is no discernible difference between the records from 527 m (Fig. 6(a)), located within the pycnocline and where the IWB can be expected to extend to $N \approx 50$ cpd, and at 700 m depth where weaker stratification is expected to support a narrower IWB (Fig. 6(b)). At 527 m a small peak in C_R is observed at M_4, rising above the background noise level but still far from the theoretical value predicted for a freely propagating internal wave. It should be noted that the variation in the position of the permanent pycnocline results in the sampling of layers of varying N including homogeneous layers of $N \sim 0$ which may dominate the internal wave spectra (van Haren, 2004b).

At moorings 1b4 and 3b4 in 600 m water depth differences are discernible between the permanent pycnocline located in the near bed region (Figs. 7(b and d), blue lines) and the weakly stratified interior at 265 m depth (Figs. 7(a and c), red lines). Whilst some peaks approaching the polarisation expected of free internal waves are found in the permanent pycnocline during both periods (Figs. 7(b and d)), they occur at non-deterministic frequencies with distinct drops in C_R in the D_4 bands and higher. In the interior however, the D_4 and D_6 frequency bands exhibit relatively broad band enhancements in C_R relative to neighboring frequencies but still failing to reach values expected of free internal waves. At 265 m the principal semidiurnal frequency band, however, is distinctly rectilinear, particularly during PROCS-1 (Fig. 7(a)). Motions over the slope in the FSC in the IWB are therefore apparently not dominated by freely propagating internal gravity waves.

3.1.3. Harmonic analysis

Tidal current ellipses computed using the harmonic analysis indicate primarily rectilinear flow as exemplified by the ellipse predicted for 700 m depth at 2b7 (Fig. 8). The orientation of currents at the specified D_2 frequencies is constant with depth at 2b7 and aligned at a heading of $27^\circ \pm 3^\circ$ relative to the long-slope direction (52°N) (Fig. 9(c)). Thus, the cross-slope velocity component, U, has typically half of the magnitude of the long-slope component, V. As suggested by the decrease in KE with depth in Fig. 3, the semi-major axes of the tidal constituents also decrease in amplitude with depth below 700 m (Fig. 9(a)). The phase relative to GMT remains constant with depth for all three major tidal constituent frequencies (Fig. 9(d)).

The shorter time-series from 1b4 and 3b4 prohibits the discrimination of the tidal constituents in the D_2 frequency band and we thus present only the results for M_2 (Figs. 9(e–h)). Currents are similar but slightly larger than those at mooring 2b7 in terms of magnitude, presumably due to the smearing of energy from neighboring tidal frequencies (particularly S_2) during the harmonic analysis. An increase in the magnitude of both the semi-major and semi-minor axes at 400–450 m depth during PROCS-3 reflects an increase in tidal current amplitude towards the top of the permanent pycnocline (Figs. 9(e and f)). The orientation of the semi-major axis is again constant with depth during both deployment periods but during PROCS-1 is within $1 \pm 18^\circ$ of the slope heading (Fig. 9(g)), a rotation of $\sim 20^\circ$ counterclockwise relative to the orientation during PROCS-3. The phase is again constant with depth (85°) for both moorings and between cruises (Fig. 9(h)). M_2 currents at b4 lead those at 850 m depth (2b7) 10 km off-shore by 20°.

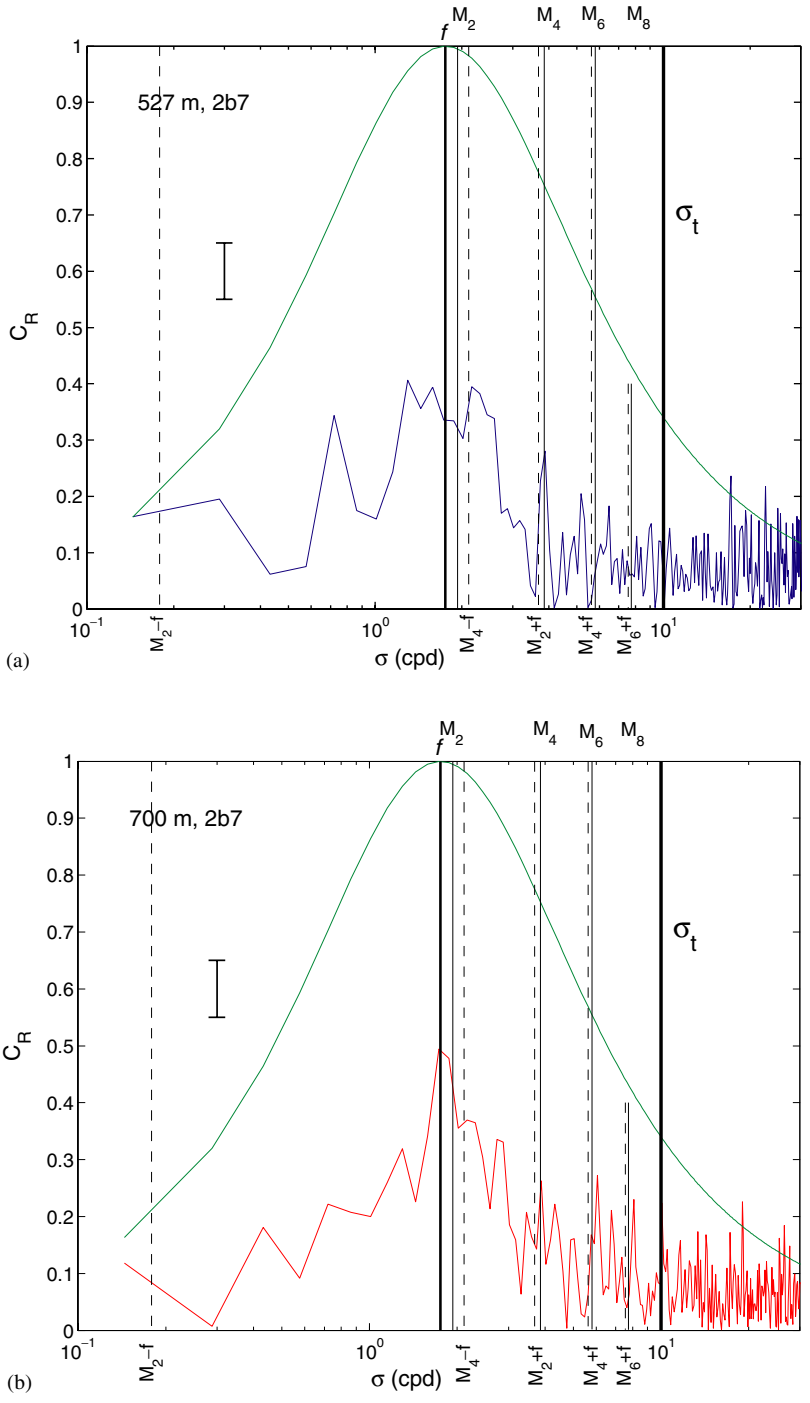

Fig. 6. Rotary coefficient, C_R, of observed currents at (a) 527 m and (b) 700 m at mooring 2b7 as calculated from Eq. (4), and the free linear internal wave solutions to Eq. (4) given by Eq. (5) (green lines). Tidal and higher harmonic frequencies and tidal–inertial interaction frequencies are indicated by black vertical solid and dashed lines, respectively and labeled accordingly.

3.2. Baroclinic currents and IT intermittency

On the basis of the results from the previous section we consider the deterministic currents at the tidal constituent frequencies to be primarily barotropic, exhibiting nearly rectilinear tidal ellipses oriented within 30° of the long-slope direction. Whilst there is a decay in current amplitude towards

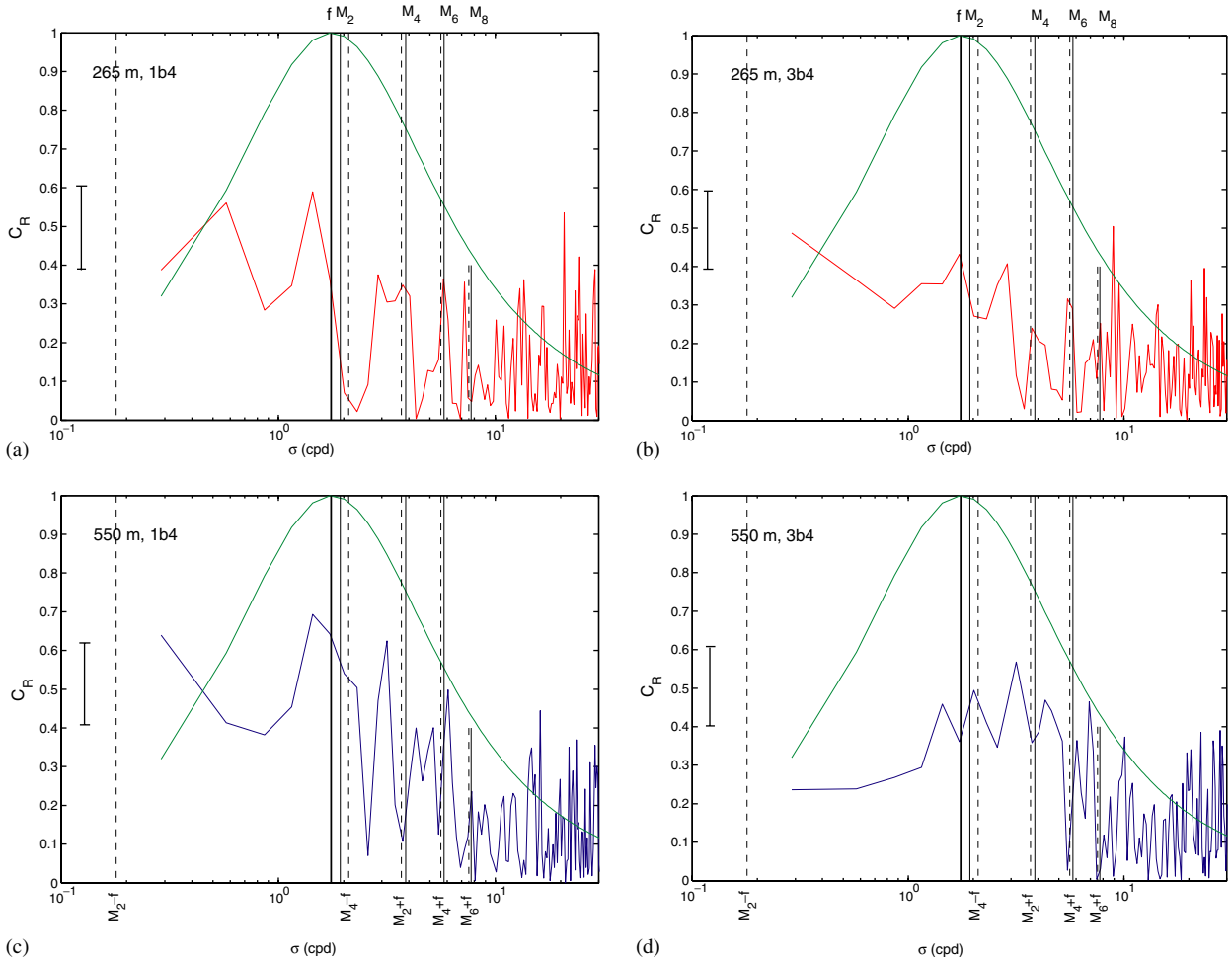

Fig. 7. As with Fig. 6 but for (a) 265 m and (b) 550 m at 1b4 and (c) 265 m and (d) 550 m at 3b4.

the sea-bed exhibited by all three principal tidal constituents, there is no accompanying phase shift in the vertical as would be expected for baroclinic tidal motions and the phase is stable between deployment periods in the source region at 600 m water depth. The absence of a phase shift across the permanent pycnocline and of a significant change in tidal current amplitude in either the source region or the far-field precludes the presence of a cIT and we thus conclude the deterministic signal to be barotropic. These conclusions are supported by those of Huthnance et al. (1988) who also found the semidiurnal currents at deterministic tidal frequencies in the FSC to be largely barotropic despite a similar decrease in amplitude towards the bottom and small variations in phase but with no apparent consistency.

Baroclinic currents in the semidiurnal frequency band, D_2, are thus defined as the residual currents, $u_1 = u - u_0$, where u is the total current in each component and u_0 is defined by Eq. (9). The baroclinic energy is smeared throughout the semidiurnal band (Fig. 10), suggestive of the non-linear interaction of deterministic tidal motions with the background conditions according to the modeled interaction between tidal and subinertial motions (van Haren, 2004a). The width of the D_2 band is defined as the frequencies at which the KE in u_1 drops to 0.1 of the peak value in the D_2 band and differs between the PP (527 m) and the interior (700 m). In the PP D_2 lies in the range $1.81 < \sigma < 2.11$ cpd; the corresponding band-width, $\Delta\sigma = 0.30$ cpd $\approx 0.15\, M_2$, indicates a period of modulation of 3.3 days. In the more weakly stratified interior the D_2 band lies in the range 1.88–2.11 cpd. The smaller bandwidth of 0.23 cpd $\approx 0.12\, M_2$ corresponds to a modulation period of 4.3 days. The KE remaining in the D_2 band following the extraction of

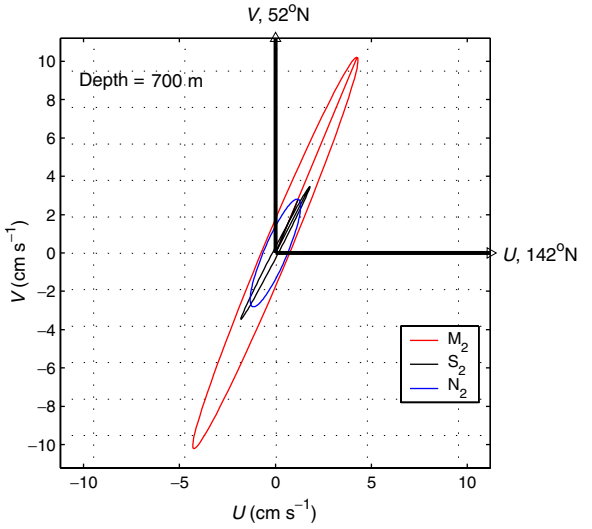

Fig. 8. Predicted current ellipses for the M_2 (red ellipse), S_2 (black ellipse) and N_2 (blue ellipse) tidal constituents determined from harmonic analysis at 700 m depth at mooring 2b7. Axes have been rotated so that the positive long-slope direction (52°N) is directly up the page and up–slope to the right.

the deterministic tidal constituents amounts to 18–20% of the total KE.

Band-passed time series of residual currents, u_1, with filter cut-offs according to the D_2 frequency range appropriate to each depth as determined from the spectra above, exhibit the familiar intermittent pulses of semi-diurnal energy (Fig. 11). At 527 m (blue lines, Figs. 11(a and d)) the number of pulses throughout the entire record corresponds to an average periodicity of 4.1 ± 0.2 days whilst at 700 m (red lines, Figs. 11(b and e)) the period increases to 5.5 ± 0.5 days. The pulses are therefore not correlated with the longer 14 days timescale of the barotropic spring-neap cycle predicted by the harmonic analysis, u_0, v_0 (Figs. 11(c and f) black lines). They appear to be slightly longer than the period expected from the residual spectra, by 0.8 days in the PP and 1.2 days in the interior but the arbitrary threshold used to define D_2 in the spectra (10% of initial energy levels) is likely to introduce some discrepancy with the timescale of the pulses observed in the time-series of baroclinic currents. The apparent discrepancy indicates a non-white icIT band which is dominated by a few peak frequencies around frequencies just off M_2 and S_2 (Fig. 10). In contrast to the barotropic tidal currents, the magnitude of the baroclinic long-slope component, v_1, is approximately equal to that of the cross-slope component, u_1, with particles describing a near-circular trajectory as opposed to the near-rectilinear paths of the barotropic semi-diurnal motions (Fig. 12). The variability in particle velocities is suggestive of different regimes dominating the records at particular times, with trajectories appearing to tend more towards those expected of free internal waves (according to Eq. (8)) at some times but becoming more rectilinear at others times. We interpret this as evidence that, at a fixed point in space, internal waves are dominant during sporadic periods, but that when averaged over the entire record the periods during which polarisations do not satisfy Eq. (8) dominate the results, thereby explaining the results of the rotary spectra which suggest that, over the whole record, freely propagating internal waves do not dominate.

3.3. Subinertial variability over the slope

Baroclinic semi-diurnal currents exhibit a subinertial modulation in intensity that is not governed by the barotropic spring–neap cycle but has an average periodicity of 3.3–4.3 days. We examine here the nature of such variability in the FSC with a view to assessing the impact of variations in the background fields on the IT behaviour. Particularly we consider how the pre-existing geostrophic balance that is observed over the Shetland slope may be perturbed, thereby eliciting changes in both stratification and low-frequency current fields.

3.3.1. Oscillatory variability in the IT source region

According to the model of Gerkema (2002) the IT is principally generated in regions where the bottom slope, α, is critical for the M_2 forcing frequency and in the overlying pycnocline. Given the relatively gentle bottom slope in the FSC, comparatively strong stratification is required to reduce the angle of the IT characteristic to one matching α with the consequence that IT generation may only occur where the permanent pycnocline (where $N^2 = O(10^{-4}\,\mathrm{s}^{-2})$) intersects the slope. Variability in the position of the pycnocline therefore, has potential implications for IT generation and the immediate path any baroclinic wave may take from the source region.

The mooring at 550 m depth during PROCS-3 is the only mooring from either cruise which was consistently located within the permanent pycnocline as inferred from the magnitude of the observed temperature gradients. Spectra of temperature

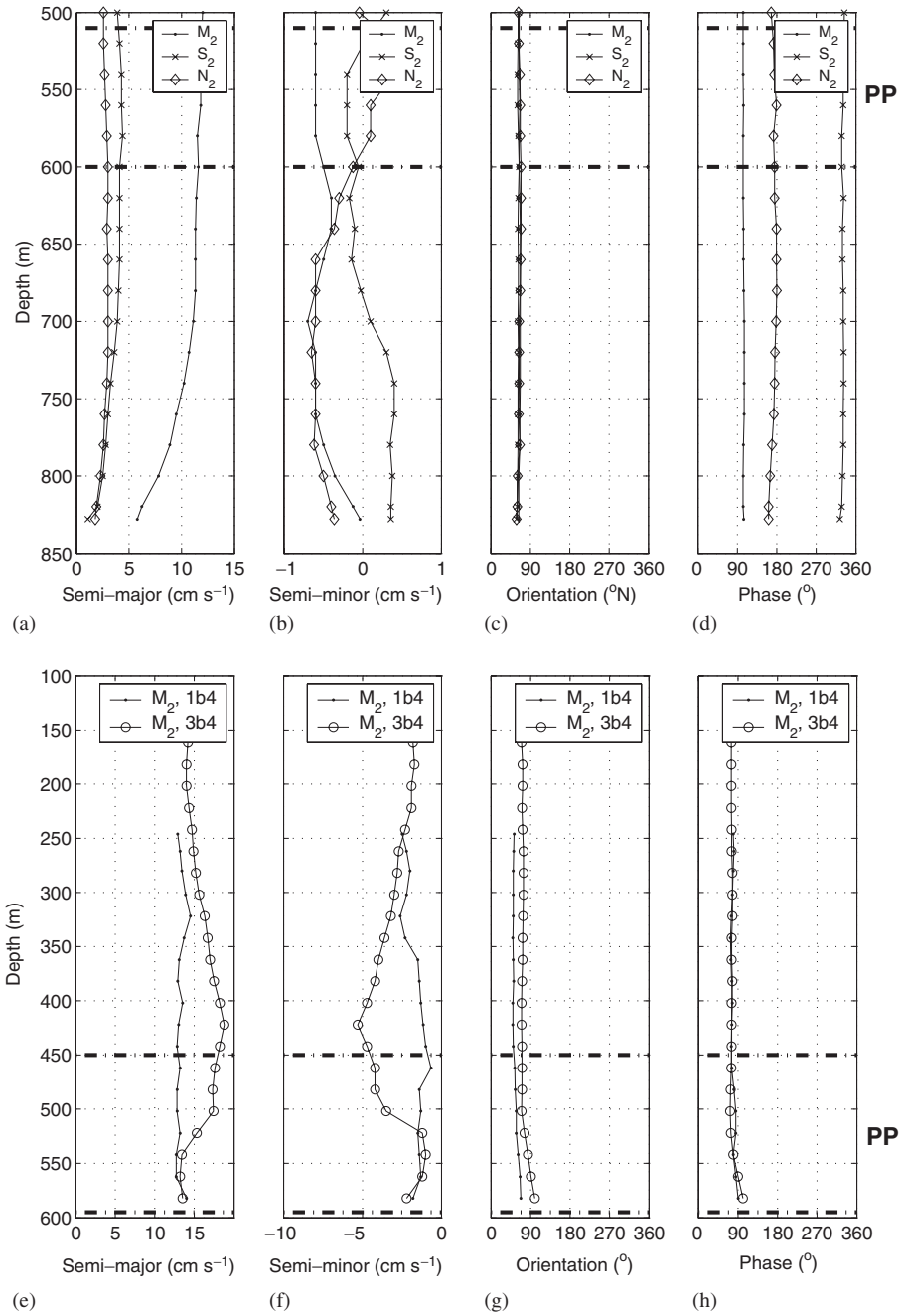

Fig. 9. Depth profiles of (a) semi-major, (b) semi-minor axes, (c) orientation and (d) phase of M_2, S_2 and N_2 tidal constituents at long-term mooring 2b7 (850 m depth) as calculated from harmonic analysis, and (e)–(h) for the M_2 constituent at short-term moorings 1b4 and 3b4 (600 m depth). Approximate positions of the permanent pycnocline (PP) are indicated by the dash–dot lines.

variance at heights above the bed, z, of 21 and 34 m reveal a broad peak at D_2 centred on M_2 and further peaks at M_4 indicating non-linearity in the M_2 tidal constituent, probably due to bottom friction given the proximity of the RCMs to the sea-bed. However, a peak at $\sigma = 0.7f$ corresponding to a period of ~20 h is also evident and with greater variance than $\sigma = M_2$ (Fig. 13(a)). Peaks at $0.7f$ are evident in temperature spectra from both current meters and are therefore not a spectral artifact of one instrument. KE spectra reveal the same peak indicating that the variance in the temperature field

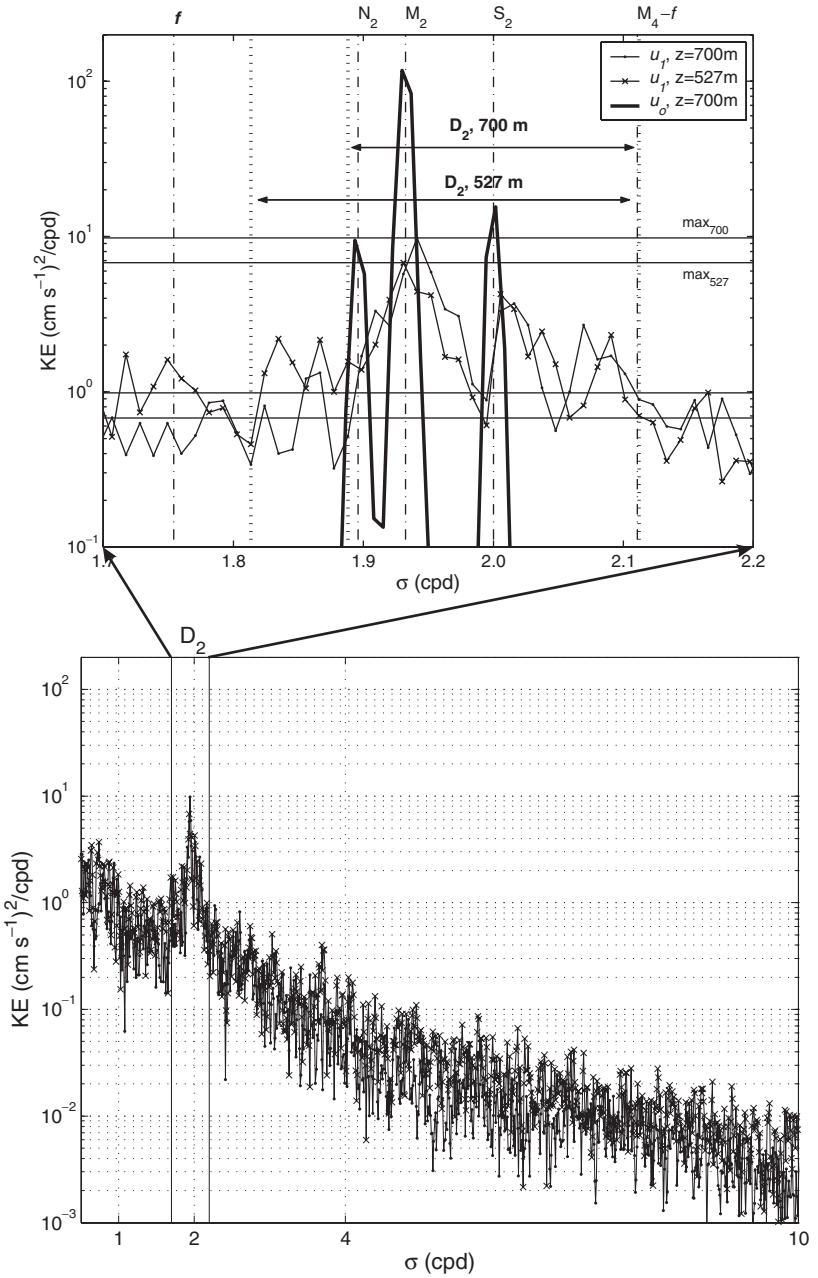

Fig. 10. (Top panel) Kinetic energy spectra of baroclinic currents, u_1 at 527 and 700 m depth at mooring 2b7 and the tidal constituents computed by harmonic analysis, u_0, which are extracted from the original time-series to form u_1. The thick black vertical lines at $\sigma = 1.81$, 1.88 and 2.11 cpd define the D_2 (semi-diurnal tidal) band at 527 and 700 m as indicated by the arrows. Horizontal lines indicate the maximum KE in the D_2 band at both 527 and 700 m and are indicated accordingly. The bottom panel indicates the an expanded portion of u_1 only at 527 and 700 m depth for $0.1 < \sigma < 10$ cpd.

is associated with fluid motions of the same periodicity. A 20-h period during days 276–277 highlighted in Fig. 13(b) indicates a complete cycle during which the temperature at $z = 21$ m ranges from 0.96 to 8.96 °C. A hodograph of band-pass filtered ($0.55f$–$0.85f$) currents for the same 20 h period describes a near-circular, clockwise rotating current ellipse (Fig. 13(c)). A spectral peak at the same frequency is not found at any of the deeper moorings which are located beneath the pycnocline.

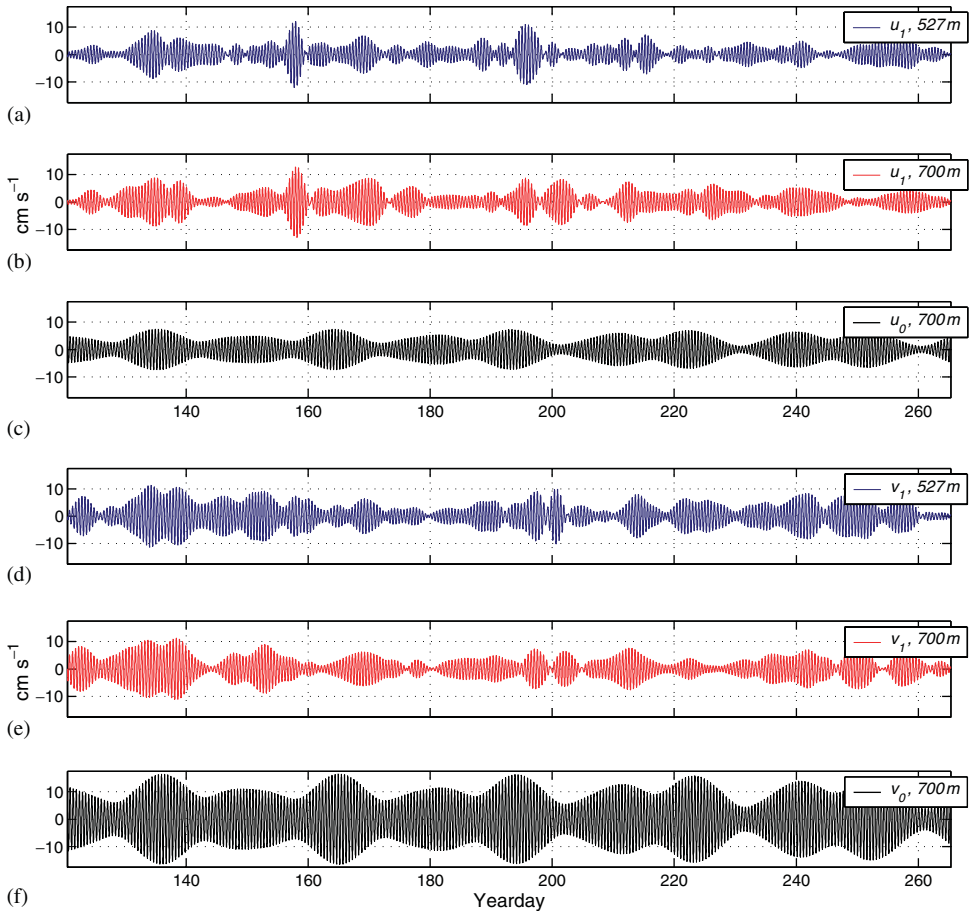

Fig. 11. D_2 band-pass filtered ($1.81<\sigma<2.11$ cpd) (a, b) cross-slope, and (d, e) long-slope baroclinic velocities, u_1, at 527 and 700 m depth at mooring 2b7, and (c) cross-slope and (f) long-slope barotropic velocities, u_0.

A frequency of $0.7f$ and clockwise rotating, circular currents correspond to the modeled form of an oscillatory continental shelf wave (CSW) in the FSC generated by short-term, impulsive atmospheric forcing (Gordon and Huthnance, 1987). The impact this motion has on the icIT is addressed in the Section 4.

3.3.2. *Quasi-steady subinertial variability over the slope*

The 3.3–4.3 day timescale of the modulation of icIT energy determined from the spectra of baroclinic currents (Fig. 10) implies a longer periodicity of motion than the oscillatory response observed at $\sigma = 0.7f$ in the previous section as being of importance to the observed icIT. Low-pass filtered (cut-off $\sigma<0.75$ cpd) currents show that both current components vary in intensity with a typical period of 4 days but are predominantly orientated in the poleward direction (Figs. 14 and 15). Velocities exceed 20 cm s^{-1} during both cruises, with long-slope currents directed predominantly poleward and tending to dominate the cross-slope component except in the interior around a depth of 200 m at the beginning of PROCS-1 (Fig. 14). On days 110 and 115 negative V (i.e. equatorward to the south-west) is observed in the lowest 50 m and an approximately 180° phase shift may be inferred with respect to the currents towards the surface; to illustrate the phase shift the (arbitrarily scaled) depth-profiles of U, V at days 113 and 115 are overlain on Figs. 14(a and b). During PROCS-3 (Fig. 15) the pulses in the low-frequency currents are equally distinct with the 180° phase difference between currents above and below the permanent pycnocline particularly evident between days 273–277.

Low-frequency temperature variability (cut-off $\sigma<0.75$ cpd) from the moorings located closest to

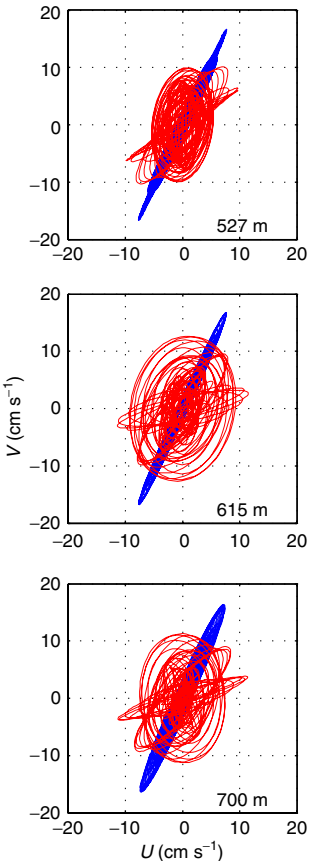

Fig. 12. Band-pass filtered ($1.81<\sigma<2.11$ cpd) hodographs of D_2 baroclinic currents, u_1, (red lines) and deterministic barotropic currents, u_0, (blue lines) for 527, 615 and 700 m depth at 2b7.

the permanent pycnocline corresponds well with the low-frequency currents and supports the notion of a timescale of variability in both the current and temperature which are commensurate with the proposed period of modulation of the IT. During PROCS-1 at 1a2 (494 m depth) the temperature is observed to drop during periods of strong poleward flow at 550 m at 1b4 (Fig. 14(d)) and, given the aforementioned 180° phase shift between the currents at 250 and 550 m, indicates that periods of maximum temperature (i.e. when the permanent pycnocline is depressed down the slope) occur when the flow at 250 m depth is poleward. The same pattern is observed during PROCS-3; maximum temperatures are observed when the current at 250 m is flowing poleward although the period at day 270 when a temperature minimum is observed at a time of strong *equatorward* flow at 550 m depth appears to be anomalous. The correspondence between low-frequency currents and temperature variance at the bed was also observed by Hosegood and van Haren (2004) who propose a quasi-periodicity of ~4 days to be related to the propagation of strong temperature fronts up the slope.

The importance of the variability of the temperature field lies in its influence on the density field, specifically the magnitude of the density variations and whether they have the potential to significantly alter the path of an internal tidal wave. We lack time-series of density measurements at a fixed point in space but profiles were taken at the same location during two CTD transects conducted 4 days apart in PROCS-1. By applying to Eq. (1) the observed values of N^2 during two profiles in 680 m water depth situated between the IT source region and the long-term mooring, 2b7, in 850 m water depth, we estimate the difference in depth through which an IT ray will pass through 2b7, 10 km off-shore of the source region (Fig. 16). The varying stratification towards the bottom (>600 m depth) and above 400 m depth causes large differences in predicted ray paths of >100 m. This naturally assumes a commensurate degree of variability in N^2 in the density field in a cross-slope direction but is consistent with the moored temperature observations which suggest the permanent pycnocline to indeed be subject to large excursions over periods of the order of 3–4 days within the short-term cruises. A definitive evaluation of the influence of variable stratification however requires an understanding of the vertical extent of the IT ray as larger spatial scales (i.e. the predominance of lower modes with greater vertical extent) are less affected by comparatively small changes in N.

4. Discussion

In the FSC icIT KE in the D_2 band amounts to 18–20% of the total signal prior to removal of the deterministic signal. Whilst kinetic energy is smeared over a frequency bandwidth $\Delta\sigma = 0.23-0.3$ cpd ($0.12–0.15\,M_2$) corresponding to a 3.3–4.3 days periodicity in the intensity of icIT currents, the largest bandwidth is found in the permanent pycnocline. This bandwidth is slightly larger than observed in the deep ocean where $\Delta\sigma = 0.09 \pm 0.02\,M_2$ or 4.7–7.4 days (van Haren, 2004a). The discrepancy between the bandwidths is most likely due to the relative proximity of the measurements to the source regions and the nature of interactions with background conditions.

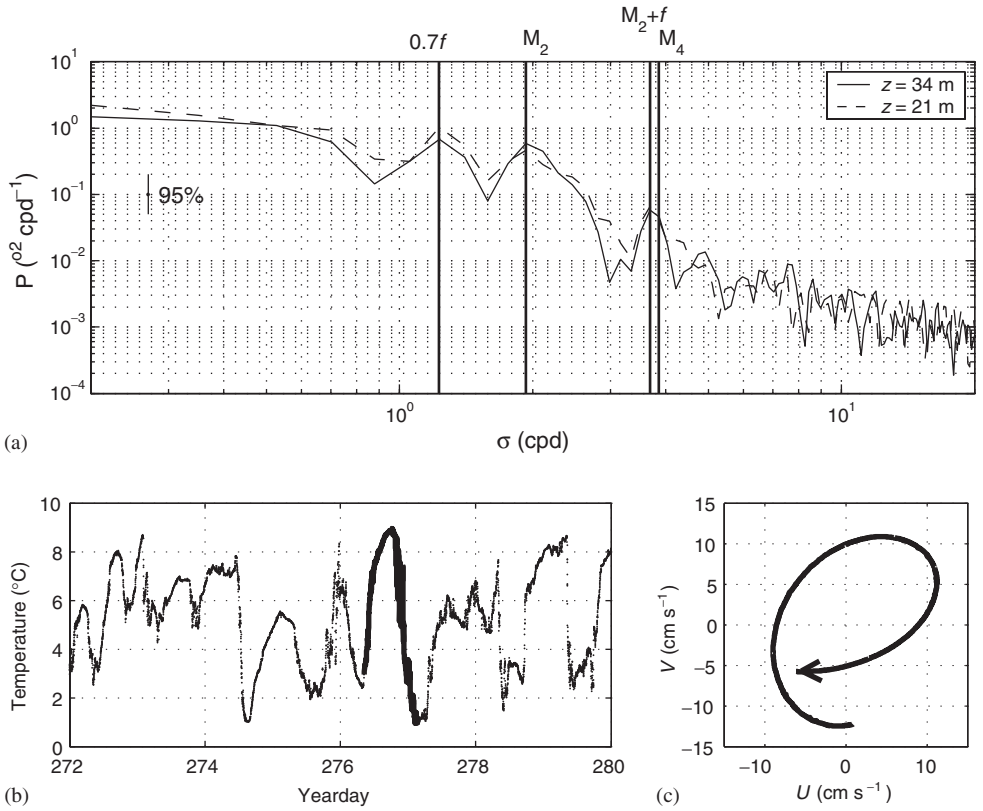

Fig. 13. (a) Temperature variance spectrum at heights above the bed, z, = 21 and 34 m at mooring 3c3 in 550 m water depth during PROCS-3, (b) the corresponding temperature time series at $z = 34$ m and (c) hodograph of band-passed ($0.55f < \sigma < 0.85f$) current during the period indicated by the solid line in (b) which represents a period of 20 h corresponding to $\sigma = 0.7f$.

4.1. The IT source region

The distinction between the IT source region at a depth of 600 m and the far-field at a depth of 850 m is corroborated by KE spectra. Fall-off rates with frequency of σ^{-3} in the KE spectra from the ADCP moored at a distance of 10 km from the predicted source of the IT in 850 m of water over the Shetland slope differ from the canonical Garrett and Munk (1972) internal gravity wave spectrum. van Haren (2004b) finds similar fall-off rates for a number of mooring sites in the eastern Atlantic and western Mediterranean and categorizes the regimes into two types; those in which the spectra are dominated at tidal and/or inertial non-linear harmonics with a σ^{-3} fall-off rate superimposed on a nearly white (noise) spectral continuum, and secondly those where the spectrum is smooth for most of the IWB outside the tidal and inertial peaks. The results presented here imply that the FSC falls into the latter category, with only a small degree of enhancement at higher harmonics. The spectrum is typical of a region subject to the non-linear dynamics that result in the peaks at higher harmonics in the former regime, but which in this case are (comparatively) far from the source (van Haren, 2004b) such that the overtides generated as free waves have moved into their own frequency space and therefore have a different angle of propagation.

The concept of a distinctly defined source region for the IT at a position over the slope where the angle of inclination of the IT matches that of the bottom slope according to Eq. (1) demands closer scrutiny. The proximity of measurements to the source region may determine their spectral characteristics and as it is clear that there is a large degree of variability in the density field it is prudent to ascertain the effect of such variability on the nature of resulting observations. If the nature of the internal wave spectrum is dependent on the proximity of the measurements to the source region

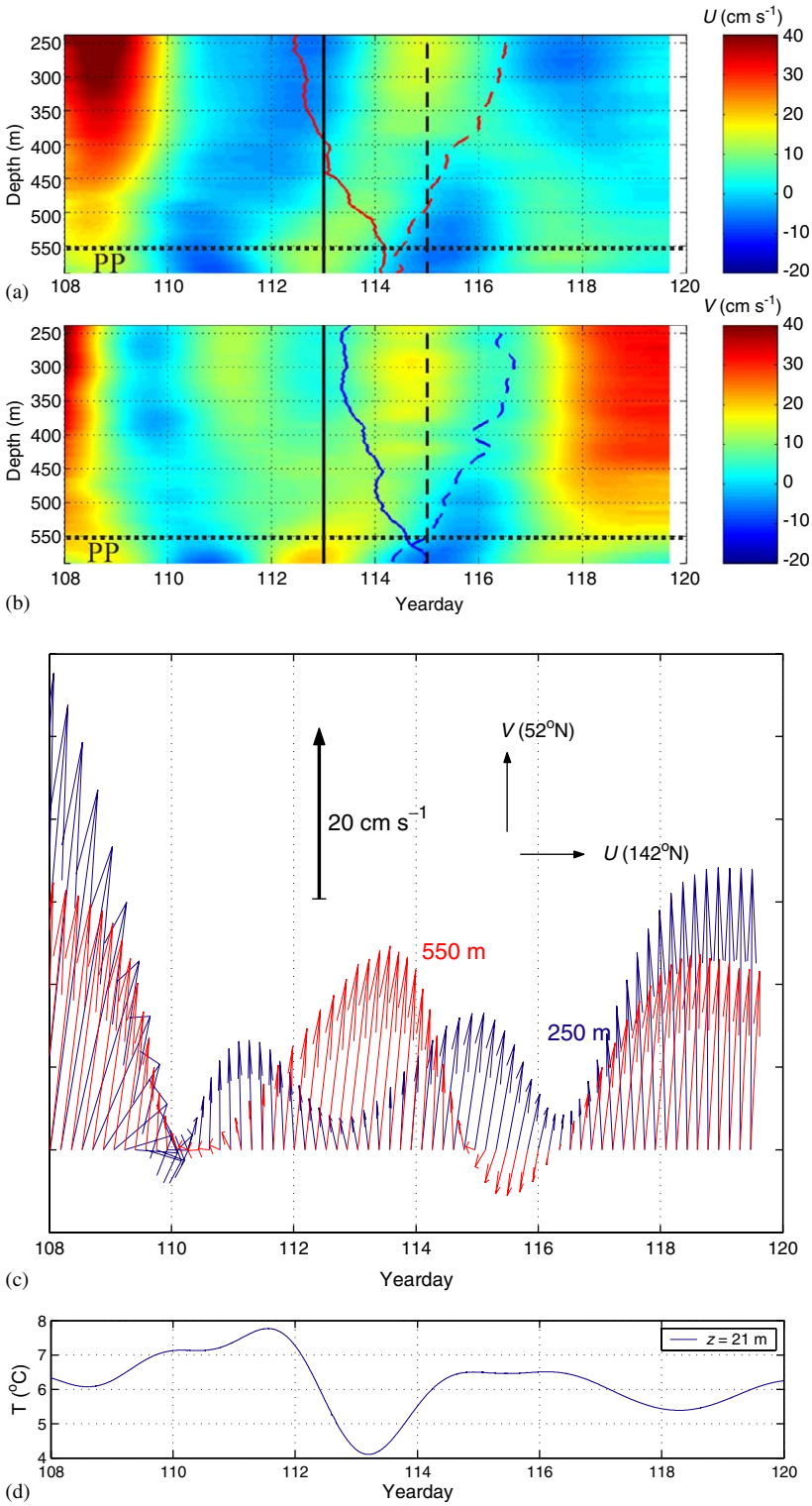

Fig. 14. Depth-time map of low pass filtered ($\sigma < 0.75$ cpd) (a) U and (b) V at mooring 1b4 and (c) corresponding quiver plots plotted at every 50th data point (~4 h), and (d) low pass ($\sigma < 0.75$ cpd) filtered temperature at $z = 21$ m, mooring 1a2 at 494 m depth. The colored solid and dashed line in (a) and (b) represent arbitrarily scaled velocities at the time indicated by the respective black vertical line. The horizontal dashed line at 550 m indicates the approximate upper edge of the PP.

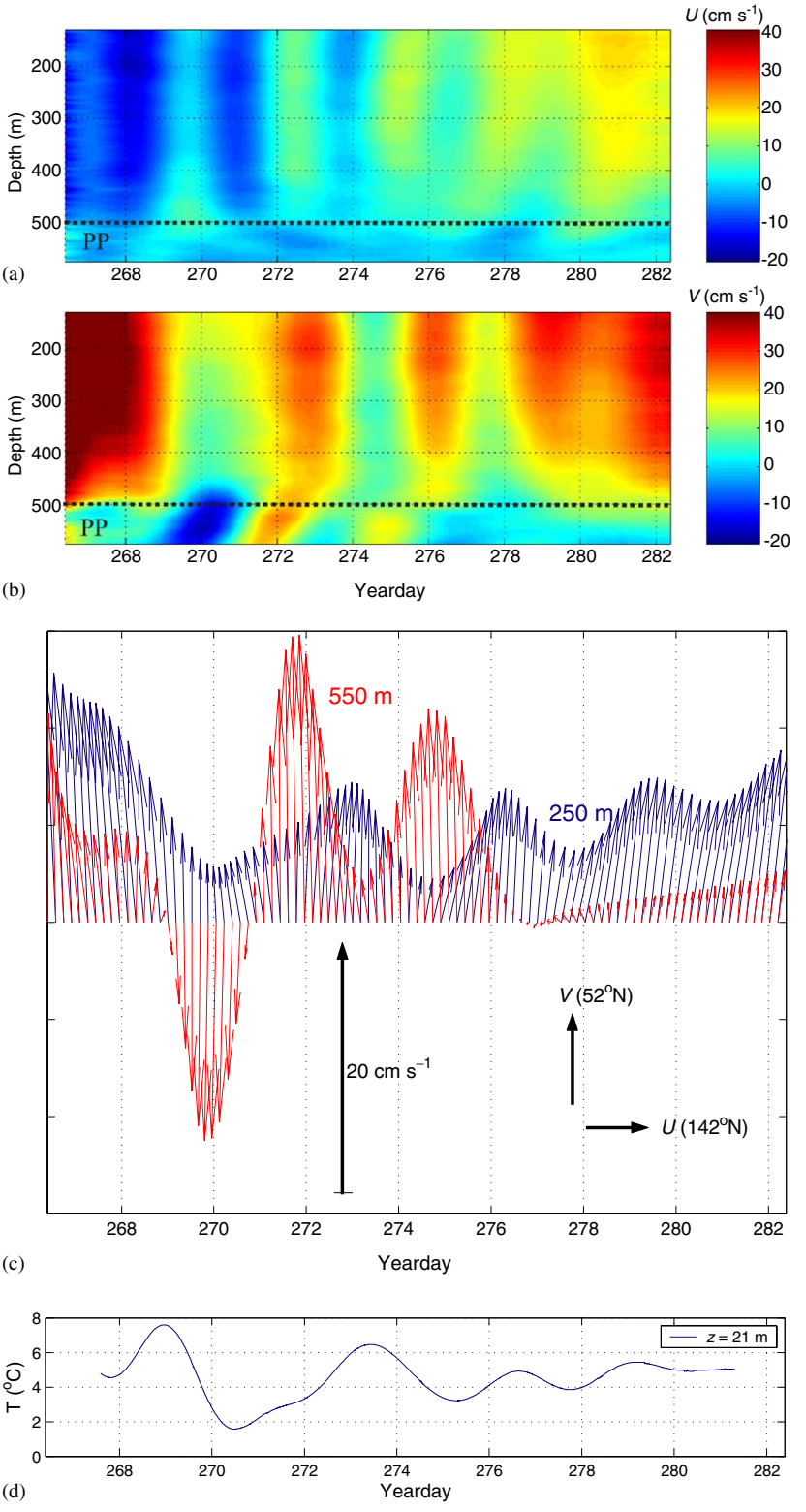

Fig. 15. As Fig. 14 for mooring 3b4 and with low-passed temperature from 3c3 at 550 m depth.

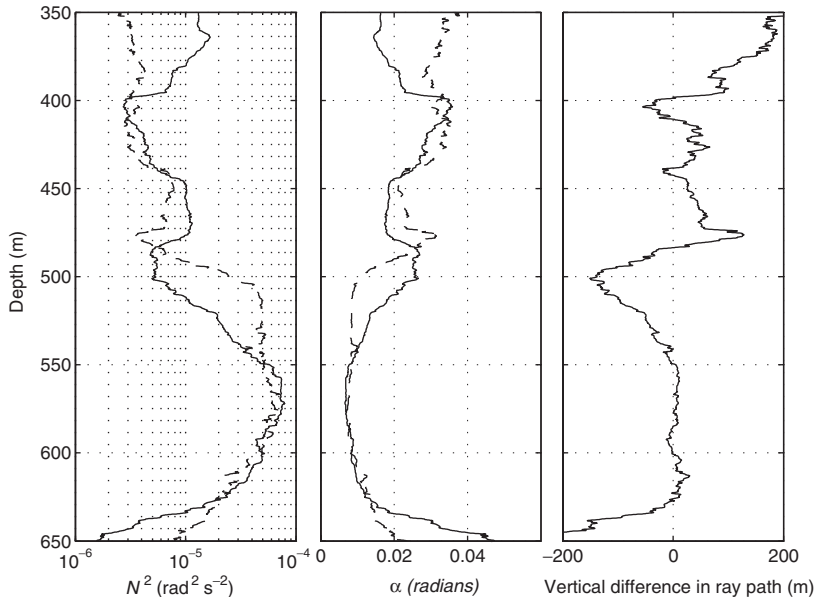

Fig. 16. (a) Buoyancy frequency, N^2 (rad^2 s^{-2}) and (b) the angle of inclination, α, of M_2 ray path according to Eq. (1) for two vertical profiles conducted 4 days apart and (c) the resulting difference in depth at which the ray would pass at a distance of 10 km off-shore due to the difference in α.

we would expect the spectra at the same depth and from the same moorings to vary on timescales commensurate with the proposed variability of the stratification amongst other factors. This appears to be the case when we consider spectra from the deeper short-term moorings, 1b7 and 3b7 in 800 m water depth and different periods of similar lengths from the long-term mooring, 2b7 nearby in 850 m water depth (Fig. 17). Despite being moored at exactly the same position in exactly the same depth of water, spectra from 600 m depth ($z = 200$ m) at 3b7 (immediately after summer) exhibit marked differences with the mooring deployed prior to summer in PROCS-1, 1b7, which reveals the presence of distinct higher tidal harmonics at M_4 and around (but not exactly at) M_6 and M_8. During PROCS-3 however all such peaks at $\sigma > M_2$ have disappeared. The absence of higher harmonics at 3b7 is not due to seasonal differences in stratification however as evidenced from the two records at 2b7. 2b7(I) represents the first 20 days of the record at 600 m depth, and thus immediately follows 1b7 in PROCS-1 and 2b7(II) represents the final 20 days of the time series immediately prior to the deployment of 3b7. In the latter, enhancement occurs at M_4 and M_6, although with the energy slightly smeared across the tidal frequencies and thus suggestive of non-linear interaction with inertial motions resulting in energy at $M_2 + f$ and $M_4 + f$. The consequence of these differences is that the character of measured spectra has a strong time dependence due to stratification varying on timescales of weeks or less. In an Eulerian frame of reference the varying background conditions will alter the path of the IT and/or the location of the non-linear interactions that generate the observed energetic peaks in the spectra. Measurements at a fixed location may simply miss the internal tidal signal from time to time, or more fundamentally the variation in the stratification varies in position with respect to the slope to the extent that it only periodically allows the generation of an IT and/or higher harmonics.

4.2. Background influences on internal wave paths

The effects of stratification and current shear, both vertical and horizontal, on the propagation of low-frequency internal waves have been studied by Mooers (1975) and Kunze (1985), the latter within the context of eddies. Mooers (1975) incorporates these effects into Eq. (1) (for a downgoing characteristic) as

$$\sin\alpha = -\frac{-M^2 - \left[M^4 + \left(\sigma^2 - f_{\text{eff}}^2\right)\left(N^2 - \sigma^2\right)\right]^{1/2}}{\left(N^2 - \sigma^2\right)}, \tag{10}$$

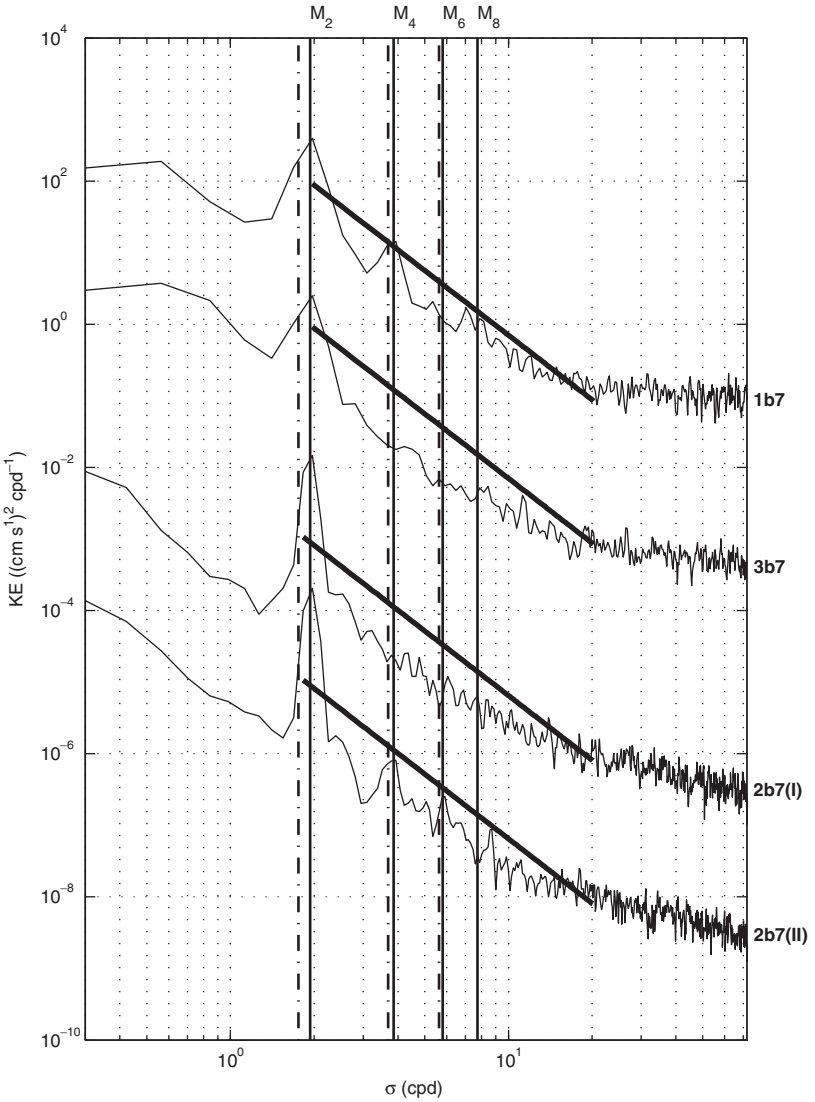

Fig. 17. Kinetic energy spectra at 600 m depth at moorings 1b7, 3b7 and for the first and last 20 days of the record at 2b7. Each record is offset by 10^{-2} from the record above. Sloping lines correspond to a σ^{-3} (solid line) and σ^{-2} (dashed line) fall-off rates and are shown for the internal wave band, $f<\sigma<N$ where $N=20$ cpd. Vertical dashed lines correspond to M_2 and its higher harmonics and the dash–dot lines to inertial, f, and its interaction frequencies.

where $f_{\text{eff}}(x,y,t)=f(f+1/2\,\zeta)$ is the effective inertial frequency, in which $\zeta=(\partial V/\partial x)-(\partial U/\partial y)$ is the low-frequency ($\sigma<0.75$ cpd) vorticity of the medium, and $M=b_x$ is the horizontal analogue of the vertical buoyancy frequency, N. The spatial and temporal dependence of N has already been discussed and we consider here the role of current variability in modulating the subinertial vorticity. Our mooring array precludes the complete determination of ζ but we are able to compute the former component, $\partial V/\partial x$, as the cross-slope gradient of the low-pass filtered ($\sigma<0.75$ cpd) long-slope velocity at the same depths between moorings 1b4 and 1b7. As with Rainville and Pinkel (2004) who studied the effects of geostrophic vorticity on internal wave propagation in the vicinity of the Kuroshio, we assume here $\partial V/\partial x \gg \partial U/\partial y$ given the observed dominance of V over U at low σ.

The modulation of the low frequency, cross-slope gradient in long-slope velocity is the dominant component in determining the vorticity but will also influence the geostrophic balance that exists in the channel over the Shetland slope. Firstly, the

boundary current and distribution of water masses within the channel cause a slope of the isopycnals upwards, away from the slope in geostrophic balance and in the correct sense for the thermal wind relation, $\partial V/\partial z = -(g/\rho_0 f)(\partial\rho/\partial x)$, where x is the cross-slope coordinate and a vertical shear in horizontal velocity exists in balance with a horizontal density gradient. In the case where the density contrast is pronounced, as in the case of the permanent pycnocline over the Shetland slope, the thermal wind relation may be discretized into $V_1 - V_2 = -(g/\rho_0 f)(\rho_2 - \rho_1)(\Delta z/\Delta x)$ (Margules, 1906), where $\Delta z/\Delta x$ is the slope of the interface and the subscripts refer to the upper and lower layers. A perturbation of the pre-existing geostrophic balance over the Shetland slope through an adjustment of $\partial V/\partial x$ requires an adjustment of the slope of the pycnocline, $\Delta z/\Delta x$ which then elevates the vertical shear, $V_1 - V_2$. The net result for internal tide propagation is that the pycnocline acts as a lens which is modified by perturbations to the geostrophic steady state and through which the IT must propagate towards the channel interior. The lens (i.e. pycnocline) is altered in terms of its stratification and slope by variations in $\partial V/\partial x$ and thus refracts the path of the IT with a timescale

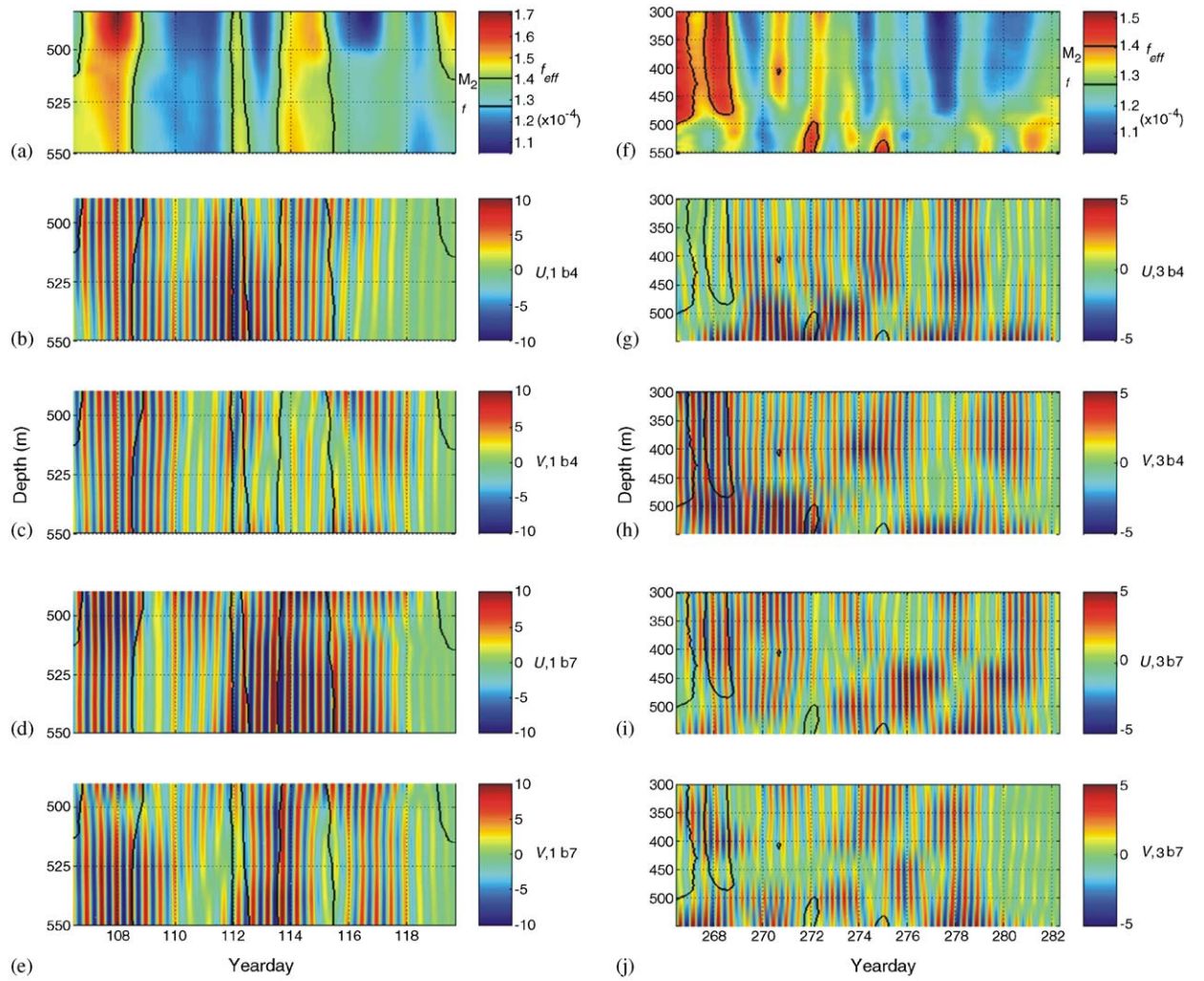

Fig. 18. Low-pass filtered ($\sigma < 0.75$ cpd) effective inertial frequency, $f_{\text{eff}} = f + 1/2\partial V/\partial x$, during (a-e) PROCS-1 (left) and (f–j) PROCS-3 (right), where $\partial V/\partial x$ is the cross-slope gradient of the long-slope velocity between the same depths at moorings b4 and b7, and (b)–(e) and (g)–(j), the band-passed D_2 icIT signal for U and V at each mooring during PROCS-1 and PROCS-3. The distance between the moorings is 8 km. Periods of $f_{\text{eff}} > M_2$ are indicated by the black contours. Note the different depth ranges during PROCS-1 (475–550 m) and PROCS-3 (300–550 m) due to the greater range of 3b7 compared to 1b7 which allowed the calculation of $\partial V/\partial x$ over a greater vertical distance during the second cruise.

commensurate with that of the modulation of $\partial V/\partial x$.

A periodicity of ~4 days is evident in $\partial V/\partial x$ with alternating positive and negative gradients such that the effective inertial frequency, f_{eff} alternates between $<f$ and $>f$ (Fig. 18). Typical gradients, $\partial V/\partial x$, between the two moorings are $\pm 2\times 10^{-5}\,\text{s}^{-1}$ corresponding to a difference in long-slope velocity between moorings of $20\,\text{cm}\,\text{s}^{-1}$. A maximum of $8\times 10^{-5}\,\text{s}^{1}$ $(=\pm 0.4f)$ on day 108 in PROCS-1 results in $f_{\text{eff}}=2.1\times 10^{-4}\,\text{s}^{-1}$. The vorticity thus easily has the potential to increase $f_{\text{eff}}>M_2$, $\left(\sigma_{M_2}=1.4\times 10^{-4}\,\text{s}^{-1}\right)$ theoretically large enough to reflect or prohibit the generation of the M_2 IT. The periods of $f_{\text{eff}}>M_2$ are indicated in Fig. 18, from which the periodicity is seen to be commensurate with the intermittency of the IT. Even allowing for the fact that some of the assumptions of Kunze (1985) are invalidated in the present case, the strong vorticity will undoubtedly cause a large degree of IT refraction between moorings b4 and b7. Its signal at a fixed point in space will therefore inevitably appear as intermittent, governed by the timescale of the motions that modulate the vorticity.

The local relation between f_{eff} and icIT energy is, however, not immediately apparent (Figs. 18). This is not surprising given the complexity of the interaction between the IT and the vorticity due to which we would not realistically expect a direct correspondence between $\partial V/\partial x$ and icIT at fixed points in space. The spatial scales relevant to the problem are not known; whilst $\partial V/\partial x$ is calculated over 10 km it is highly unlikely that the velocity gradient in the cross-slope direction is uniform and smaller scales in $\partial V/\partial x$ of which we have incomplete knowledge will undoubtedly alter the IT paths (Note: Oey (1998) proposes that a spatial resolution of 2 km is required to adequately model the eddy fields in the FSC which result from large-scale wind forcing). We furthermore do not know the vertical scale of the IT itself and therefore to what extent it is subject to variations in $\partial V/\partial x$. Smaller scales will be more strongly affected by background variations in an analogous manner to the preferential damping of higher modes (Wunsch, 1975). From a temporal perspective it is not apparent on what timescales the response of the icIT to variations in the background fields would manifest itself. Patterns do emerge however which suggest that the low-frequency vorticity does influence the intensity of the icIT and on timescales that are in accordance with the previously suggested 3–4 days periodicity in icIT. During PROCS-1 (Figs. 18(a–e)) the band-pass filtered $(1.81<\sigma<2.11\,\text{cpd})$ baroclinic long-slope velocity, V, is inhibited at 1b4 on day 114 and on day 115 at 1b7 during a period of enhanced f_{eff}. In contrast however the cross-slope velocities appear to be intensified during the period when f_{eff} is sufficiently large to theoretically prohibit the generation or propagation of the M_2 IT. During PROCS-3 the greater vertical coverage illustrates the vertical variability in icIT energy. The alternating periods of enhanced icIT energy broadly correspond to the pattern of f_{eff} such that the larger tidal amplitudes coincide with periods of negative $\partial V/\partial x$ (i.e. $f_{\text{eff}}<f$), particularly during the second half of the record when icIT intensity varies on either side of the permanent pycnocline (at approximately 500 m depth) as inferred from the vertical structure of f_{eff}. A direct comparison of the icIT response to varying f_{eff} clearly requires a fuller understanding of the initial IT behaviour and an accurate knowledge of the entire background fields, both density and vorticity.

4.3. Source of subinertial variability in background fields

Whilst we have observed significant subinertial variability in the density and velocity fields that have the potential to significantly alter the path of the IT, a significant step is to determine the cause of the background variations. Previous work in the region suggested the observed 4-day period between the occurrence of near-bed solibores to be related to atmospheric forcing which is strong and has a similar timescale in the FSC (Hosegood and van Haren, 2004). We propose this source of the subinertial variability over the continental slope in the FSC to be CSWs. Two responses to meteorological forcing have been modelled by Gordon and Huthnance (1987) for the FSC; the first is an oscillation with $\sigma=0.6f$, clockwise rotating currents and resulting from short impulsive wind events, whilst the second is a 'quasi-steady' response which arises from stronger wind events of longer duration and causes an along-isobath current that flows as long as the wind blows. Evidence for both responses is found in the current and temperature variability throughout PROCS; temperature spectra from 550 m depth during PROCS-3 revealed a peak at $\sim 0.7f$, consistent with the frequency of the response imposed by impulsive winds and

corresponding to a period of ~20 h. Temperature time-series reveal oscillations with the same periodicity and concurrent band-passed ($0.55f < \sigma < 0.85f$) currents describing circular, clockwise motion. No moorings were located in the region of maximum temperature gradients (i.e. the permanent pycnocline) during PROCS-1 and thus the temperature spectra fail to exhibit a peak at the same frequency. Whilst we lack the wind data to correlate with those of the currents, previous results have alluded to such a coupling between meteorological forcing, principally long-slope winds, and the oceanic response in the form of first-mode CSWs (Huthnance et al., 1988). The relatively short timescale of the oscillatory response is not expected to significantly alter the propagation of the IT but appears to be important in modulating the position and intensity of the stratification over the Shetland slope where the IT may be generated given the observed variability in temperature at 550 m depth at a frequency of $0.7f$ and which is indicative of variability in the position of the pycnocline.

The lower-frequency response ($\sigma < 0.5$ cpd) to more persistent wind forcing, particularly longshore wind stress which has been stated by Huthnance et al. (1986) as being most effective for generating shelf waves adjacent to a coast, is implied by the time scale of variability of the low-frequency current variability and its long-slope predominance on time scales consistent with the passage of atmospheric storms through the region. The response is referred to by Gordon and Huthnance (1987) as the 'quasi-steady response'. It should be noted that the periodicity of this response is variable and thus not a periodicity with a deterministic frequency but is rather quasi-periodic with a timescale set by the atmospheric forcing. Again we lack wind stress data but hindcast model results indicate a periodicity of approximately 4 days in the passage of storms through the study region (see Hosegood and van Haren, 2004 for details). Direct measurements were made by the R.V. *Pelagia* which was located on a storm track on days 110 and 111 during PROCS-1. Wind stress ≈ 1 Pa throughout day 110 and into 111, at which time low-frequency V increases towards the surface before appearing to penetrate down to the sea-bed causing the maximum at 550 m depth on day 112–113 (Fig. 14). The magnitude of the current velocity is entirely consistent with the magnitude of the forcing according to the model of Gordon and Huthnance (1987) which predicts a response ratio of current magnitude to the imposed wind stress of $0.2\,\mathrm{ms^{-1}\,Pa^{-1}}$ as observed between days 111 and 114. Furthermore, the magnitude of $\partial V/\partial x$ between moorings is entirely consistent with the off-shore decay of V predicted by Gordon and Huthnance (1987) at the position over the slope where our observations were made. The model predicts an off-shore decay in V of $\sim 20\,\mathrm{cm\,s^{-1}}$ between the position of our mooring at 600 m depth and the mooring at 800 m depth (Fig. 13(a), GH87), further indicating that the magnitude of $\partial V/\partial x$ which we observe is remarkably similar to that expected due to the quasi-steady, low-frequency response of CSW to wind forcing. The quasi-steady response is not unique to the model above; similar quasi-steady responses to wind forcing have been proposed by Csanady (1998) and Brink and Allen (1998) whereby a non-wavelike response to suddenly applied along-slope wind arises. The non-wavelike flow is necessary in the presence of friction to take over the role of coastal jets that would otherwise balance the off-shore Ekman transport that results from the along-slope wind stress (Csanady, 1998). Observational evidence supports the role played by low-frequency CSW response to wind forcing. Skagseth and Orvik (2002) determine that fluctuations in the Norwegian Atlantic slope current are the result of CSWs propagating along the slope in the manner described by Gordon and Huthnance (1987), with the most prominent periods determined by EOF decomposition to be 3–5 days, in good agreement with the results presented here.

Gordon and Huthnance (1987) consider only barotropic motions whilst we may expect the stratification of the permanent pycnocline to induce baroclinic motions. The influence of stratification is expressed though the parameter $S \equiv N^2H^2/f^2L^2$, where H is total water depth and L is the cross-slope scale (Huthnance et al., 1986). For moderate $N^2 = 1 \times 10^{-5}\,\mathrm{s^{-2}}$, $H = 1$ km and $L = 35$ km, $S = 0.5$ which means stratification is of minor importance; observations indicate $N^2 \to 1 \times 10^{-4}\,\mathrm{s^{-2}}$ at times over the slope however, increasing S by an order of magnitude within the permanent pycnocline and implying baroclinic motions in the near-bed region where the intense motions are observed at b4 (particularly 3b4) and which are approximately 180° out of phase with the surface currents as expected for mode 1 baroclinic internal Kelvin waves (Huthnance, 1981). Thus, despite the shelf being much wider than the internal deformation radius, $R_i = NH/f = 7.5$ km, in the more weakly stratified parts of the channel, the enhanced

stratification within the permanent pycnocline may result in $R_i > L$ such that the slope is 'seen' as a coastal wall and the waves tend to internal Kelvin-like waves (Huthnance et al., 1986). In the case of the FSC, where the stratification is comparatively strong and separates two weakly stratified regions, a combination of barotropic and baroclinic components may form the response to along-slope wind forcing in the manner described by Allen (1976); a definitive evaluation of the role played by stratification in modifying the form of CSWs is however beyond the scope the current paper.

It is important to stress that a lack of data in the long-slope direction for the current study prohibits a determination of the along-slope properties of the subinertial variability, specifically the propagation speed, c, and the along-slope wavenumber, k. We therefore cannot compare the observations to a theoretical dispersion relation for CSW with frequency, $\omega(k) = 2bk/(k^2 + b^2 + n^2\pi^2)$, where b is the (non-dimensional) shelf slope, k is along-slope wavenumber and n is the mode number (Gordon and Huthnance, 1987). It is, however, relevant to point out that the two CSW responses discussed here come from two different points on the dispersion curve for a mode 1 response, with the first representing the low-frequency, quasi-steady response in the low-k, non-dispersive regime in which the group velocity travels in the same sense as for an internal Kelvin wave (i.e. shallow water to the right in the northern hemisphere). Currents tend to follow isobaths, in direct contrast to the second response corresponding to the non-propagating, zero group velocity, maximum (and resonant) frequency regime in which the cross-slope currents approach the same size as the along-slope velocity component. In the latter case, energy remains trapped in the forcing region after energy at other frequencies has propagated away and the oscillatory motion is observed, whilst the low-frequency response propagates slowly in the along-slope direction in geostrophic balance with the cross-slope pressure gradients (Csanady, 1997). The quasi-steady response will thus require additional data from much further along the slope in any attempt to identify its structure and propagation characteristics, but its perturbation of the vorticity field through its influence on $\partial V/\partial x$, whilst maintaining the overall geostrophic balance (but obviously an adjusted state of geostrophic balance relative to that prior to the wind forcing) remains a strong candidate for modulating the path of the IT and determining its intermittency. Furthermore, a correlation with wind stress is necessary to identify the role of CSWs but will be difficult to achieve. It is likely that the spatial extent of the wind stress, its orientation with respect to the slope, its duration and intensity will be important factors to account for and to measure all such variables is far beyond the scope of the current paper.

Whilst CSWs remain the most likely mechanism for modulating the background environment, both that of low-frequency vorticity and of stratification, it is prudent to briefly consider alternative mechanisms that may perturb the environment over the Shetland slope in a manner that could influence IT propagation. Barotropic instability of the slope current may develop into meanders and eventually eddies (Huthnance, 1995), whilst Mysak and Schott (1977) propose baroclinic instability to be responsible for a 2–3 days fluctuation in the Norwegian Current. The parameters employed in their model are very similar to those appropriate for the FSC but we note that the velocity differences between the upper and lower layers may also represent $\partial V/\partial x$ in a two-layer system in which the interface is sloping, as is the case in the FSC. Given the results of Skagseth and Orvik (2002) who explain the fluctuations as CSW with the benefit of observations of wind stress, we propose that the same wind forcing is dominant in the FSC given the adherence of our results with the CSWs of Gordon and Huthnance (1987). Eddies are thought to propagate along the Shetland slope with a periodicity of approximately 8 days which is too long to explain our observations, despite the proposition of Chapman and Brink (1987) that eddies compressed against the slope will induce strong along-slope flow which could feasibly contribute to variability in $\partial V/\partial x$. We propose that, until further evidence is obtained, CSW propagation along the slope is the most likely mechanism generating the modulation of the background conditions due to their cross-slope gradients in V which, in addition to influencing the low-frequency vorticity to the extent that the M_2 IT is unable to propagate, also elicits a geostrophic adjustment of the permanent pycnocline which further refracts the IT. We note however that CSW propagation may provide the impetus to generate the barotropic instability that may subsequently develop into the meanders and eddies that are known to exist in the channel such as those demonstrated by Oey (1998).

5. Conclusions

Kinetic energy spectra measured in the weakly stratified interior and the permanent pycnocline in 850 m water depth over the continental slope in the Faeroe-Shetland Channel (FSC) are relatively smooth in the internal wave band with a fall-off rate with frequency of σ^{-3}. The large fall-off rate as compared to the GM spectrum is indicative of a regime in which the IWB is dominated by higher harmonics as a result of non-linear advection occurring far from the measurement location, resulting in the broadening of the higher harmonic frequency bands and the further smearing of energy to non-tidal constituent frequencies. In shallower water higher up the slope a σ^{-2} fall-off rate results from the passage of strongly non-linear fronts through the mooring, complimenting previous observations in the study region in which the permanent pycnocline evolves nonlinearly during up–slope surges and further indicating the susceptibility of the spectral slope to its proximity to the source of such non-linear interactions. The temporal variability in the location of the non-linear interactions is evident from spectra computed for the same location but at different periods, with varying spectral slopes and energy levels at interaction frequencies depending on the time at which measurements were made.

Motions at deterministic semidiurnal (D_2) tidal frequencies are predominantly barotropic. The incoherent internal tide (icIT), defined as the residual currents after extracting the deterministic motions, is intermittent when observed in 850 m water depth, approximately 10 km offshore of the internal tide (IT) source region. Pulses of semidiurnal tidal energy occur with an average periodicity of 3.3–4.3 days in the permanent pycnocline and weakly stratified interior respectively, commensurate with the width of the D_2 band, $\Delta\sigma = 0.23-0.3$ cpd, across which the energy is smeared out of the dominant M_2 tidal constituent.

The background conditions that determine the subinertial variability of the IT are the density field and the low-frequency vorticity. The former is observed during short-term deployments to vary over a timescale of, typically, 3–4 days to the extent that changes in the buoyancy frequency at a fixed point in space may explain vertical shifts of >100 m in the position at which an internal wave ray passes through a mooring at a distance of approximately 10 km from the source region. Computations of one component of the vorticity, ζ, indicate the potential of cross-slope gradients in the low-frequency long-slope velocity component, $\partial V/\partial x$, to increase the effective Coriolis frequency above that of the semidiurnal tide, thereby (theoretically) prohibiting the generation of or reflecting the IT. The low-frequency vorticity easily has the capability to significantly refract the path of the IT, probably to a greater extent than the variability in the density field. $\partial V/\partial x$ also varies with a subinertial periodicity of 3–4 days which is consistent with the observed bandwidth of the D_2 frequency band. Low-pass filtered velocities indicate the same periodicity at the mooring deployed at a depth of 600 m in the IT source region, with a 180° phase shift between currents near the surface and those near the bottom.

The source of the subinertial variability in the background conditions is proposed to be continental shelf waves (CSWs), generated by longshore wind stress. The observed currents are consistent with previous modeling studies which propose two types of CSW response to meteorological conditions in the FSC; under short impulsive wind events, clockwise rotating currents with $\sigma = 0.7f$ are observed whilst stronger wind events of longer duration cause a 'quasi-steady' response with an along-isobath current that flows as long as the wind blows. The low-frequency response propagates slowly along the slope in geostrophic balance but perturbs the pre-existing geostrophic balance. The region of altered stratification and low-frequency vorticity, in addition to the modified slope of the pycnocline, therefore act as a lens to the IT, dramatically influencing its ability to propagate into the channel interior. In the specific case of the FSC, the enhanced stratification in the permanent pycnocline results in a baroclinic component, and therefore vertical structure, in the CSWs as opposed to the purely barotropic, depth-independent motion predicted in the modelling study.

Acknowledgments

The data were acquired during the Processes on the Continental Slope (PROCS) project, funded by the Netherlands Organisation for the Advancement of Scientific Research (NWO). We thank the Department of Sea Technology for the preparation of the moorings and the crew of the R.V. *Pelagia* for their assistance during their deployment and recovery. We further thank Theo Hillebrand for his

careful and thorough preparation of the instrumentation. Two reviewers provided thorough and useful comments which have improved the paper and we thank them for their time and effort.

References

Allen, J.S., 1976. Some aspects of the forced wave response of stratified coastal regions. Journal of Physical Oceanography 6, 113–119.

Baines, P.G., 1982. On internal tide generation models. Deep-Sea Research 29 (3A), 307–338.

Brink, K.H., Allen, J.S., 1998. Comments on 'The non-wavelike response of a continental shelf to wind' by G.T. Csanady. Journal of Marine Research 56, 789–792.

Chapman, D.C., Brink, K.H., 1987. Shelf and slope circulation induced by fluctuating offshore forcing. Journal of Geophysical research 92 (C11), 11,741–11,759.

Csanady, G.T., 1997. On the theories that underlie our understanding of continental shelf circulation. Journal of Oceanography 53, 207–229.

Csanady, G.T., 1998. The non-wavelike response of a continental shelf to wind. Journal of Marine Research 56, 773–788.

Cummins, P., Cherniawksi, J.Y., Foreman, M.G.G., 2001. North Pacific internal tides from the Aleutian Ridge: altimeter observations and modeling. Journal of Marine Research 59, 167–191.

deWitt, J.M., Levine, M.D., Paulson, C.A., Burt, W.V., 1986. Semidiurnal internal tide in JASIN: observations and simulation. Journal of Geophysical Research 91 (C2), 2581–2592.

Dronkers, J.J., 1964. Tidal Computations in Rivers and Coastal Waters. North Holland, Amsterdam.

Dushaw, B.D., Cornuelle, B.D., Worcester, P.F., Howe, B.M., Luther, L.S., 1995. Barotropic and baroclinic tides in the central north Pacific Ocean determined from long-range reciprocal acoustic transmissions. Journal of Physical Oceanography 25, 631–647.

Eich, M.L., Merrifield, M.A., Alford, M.H., 2004. Structure and variability of semidiurnal internal tides in Mamala Bay, Hawaii. Journal of Geophysical Research 109, C05010.

Ekman, V.W., 1931. On internal waves. Rapports et Proces-Verbaux des Reunions du Conseil Permanent International pour 1' Exploration de la Mer 76, 5–34.

Garrett, C.J.R., Munk, W.H., 1972. Space–time scales of internal waves. Geophysical Fluid Dynamics 3, 225–264.

Gerkema, T., 2001. Internal and interfacial tides: beam scattering and local generation of solitary waves. Journal of Marine Research 59, 227–251.

Gerkema, T., 2002. Application of an internal tide generation model to baroclinic spring–neap cycles. Journal of Geophysical Research 107 (C9), 3124.

Gonella, J., 1972. A rotary-component method for analyzing meterological and oceanographic vector time series. Deep-Sea Research 19, 833–846.

Gordon, L.E., Huthnance, J.M., 1987. Storm-driven continental shelf waves over the Scottish continental shelf. Continental Shelf Research 7 (9), 1015–1048.

Hackett, B., Røed, L.P., 1998. A numerical study of the slope current northwest of the British Isles. Continental Shelf Research 18, 1–30.

Hosegood, P.J., van Haren, H., 2003. Ekman-induced turbulence over the continental slope in the Faeroe-Shetland Channel as inferred from spikes in current meter observations. Deep-Sea Research I 50, 657–680.

Hosegood, P.J., van Haren, H., 2004. Near-bed solibores over the continental slope in the Faeroe-Shetland Channel. Deep-Sea Research II 51, 2943–2971.

Hosegood, P.J., van Haren, H., Veth, C., 2005. Mixing in the interior of the Faeroe-Shetland Channel. Journal of Marine Research 63 (3), 529–561.

Huthnance, J.M., 1981. Waves and currents near the continental shelf edge. Progress in Oceanography 10, 193–226.

Huthnance, J.M., 1989. Internal tides and waves near the continental shelf edge. Geophysical and Astrophysical Fluid Dynamics 48, 81–106.

Huthnance, J.M., 1995. Circulation, exchanges and water masses at the ocean margin: the role of physical processes at the shelf edge. Progress in Oceanography 35, 353–431.

Huthnance, J. M., Mysak, L. A., Wang, D-. P., 1986. Coastal trapped waves. In: Mooers, C.N.K. (Ed.), Baroclinic Processes on Continental Shelves. American Geophysical Union, Washington, DC.

Huthnance, J. M, Loynes, J., Edden, A. C., 1988. An investigation of meteorological effects on currents in the shelf and continental slope seas northwest of the UK. I. Analysis for individual moorings. Oceanographic Laboratory Report no. 2, 211pp.

Kunze, E., 1985. Near-inertial wave propagation in geostrophic shear. Journal of Physical Oceanography 15, 544–565.

Lam, F.-P.A., Maas, L.R.M., Gerkema, T., 2004. Spatial structure of tidal and residual currents as observed over the shelf break in the Bay of Biscay. Deep-Sea Research I 51, 1075–1096.

Lien, R.C., Gregg, M.C., 2001. Observations of turbulence in a tidal beam and across a coastal ridge. Journal of Geophysical Research 106, 4391–4575.

Maas, L.R.M., Benielli, D., Sommeria, J., Lam, F.-P.A., 1997. Observation of an internal wave attractor in a confined, stably stratified fluid. Nature 388, 557–561.

Margules, M., 1906. Uber temperaturschitchung in stationar bewegter und ruhender Luft. Meterologische Zeifschrift 23, 243–254.

Mooers, C.N.K., 1975. Several effects of a baroclinic current on the cross-stream propagation of inertial-internal waves. Geophysical Fluid Dynamics 6, 245–275.

Mysak, L.A., Schott, F., 1977. Evidence for baroclinic instability of the Norwegian Current. Journal of Geophysical Research 82 (15), 2087–2095.

Nash, J.D., Kunze, E., Toole, J.M., Schmitt, R.W., 2004. Internal tide reflection and turbulent mixing on the continental slope. Journal of Physical Oceanography 34, 1117–1134.

Oey, L.Y., 1998. Eddy energetics in the Faroe-Shetland channel: a model resolution study. Continental Shelf Research 17 (15), 1929–1944.

Pingree, R.D., New, A.L., 1991. Abyssal penetration and bottom reflection of internal tidal energy in the Bay of Biscay. Journal of Physical Oceanography 21 (1), 28–39.

Prinsenberg, S.J., Wilmot, W.L., Rattray, M., 1974. Generation and dissipation of coastal internal tides. Deep-Sea Research 21, 263–281.

Rainville, L., Pinkel, R., 2004. Observations of energetic high-wavenumber internal waves in the Kuroshio. Journal of Physical Oceanography 34, 1495–1505.

Ray, R.D., Cartwright, D.E., 2001. Estimates of internal tidal energy fluxes from Topex/Poseidon altimetry: central North Pacific. Geophysical Research Letters 28, 1259–1262.

Ray, R.D., Mitchum, G.T., 1997. Surface manifestation of internal tides in the deep ocean: Observations from altimetry and island gauges. Progress in Oceanography 40, 135–162.

Schott, F., 1977. On the energetics of baroclinic tides in the North Atlantic. Annales Geophysicae 33, 41.

Sherwin, T.J., Turrell, W.R., Jeans, D.R.G., Dye, S., 1999. Eddies and a mesoscale deflection of the slope current in the Faroe-Shetland Channel. Deep-Sea Research I 46, 415–438.

Sjoberg, B., Stigebrandt, A., 1992. Computations of the geographical distribution of the energy flux to mixing processes via internal tides and the associated vertical circulation in the ocean. Deep-Sea Research 39 (2), 269–291.

Skagseth, Ø., Orvik, K.A., 2002. Identifying fluctuations in the Norwegian Atlantic Slope Current by means of empirical orthogonal functions. Continental Shelf Research 22, 547–563.

Smyth, R., 1995. Currents on the West Shetland continental slope. M.Sc Thesis, School of Ocean Sciences, University of Wales, Bangor, p. 83.

STRATEGEM Partners, 2003. Stoker, M.S. (Compiler). Neogene evolution of the glaciated European margin. A product of the EC-supported STRATEGEM Project. World Wide Web Address: http://www.strategem-europe.org

Turrell, W.R., Slesser, G., Adams, R.D., Payne, R., Gillibrand, P.A., 1999. Decadal variability in the composition of Faeroe-Shetland Channel Bottom Water. Deep-Sea Research I 46, 1–25.

van Haren, H., 2003. On the polarization of oscillatory currents in the Bay of Biscay. Journal of Geophysical Research 108 (C9), 3290.

van Haren, H., 2004a. Incoherent internal tidal currents in the deep ocean. Ocean Dynamics 54, 66–76.

van Haren, H., 2004b. Some observations of nonlinearly modified internal wave spectra. Journal of Geophysical Research 109, C03045.

van Haren, H., Groenewegen, R., Laan, M., Koster, B., 2001. A fast and accurate thermistor string. Journal of Atmospheric Oceanic Technology 18, 256–265.

van Raaphorst, W., Malschaert, H., van Haren, H., Boer, W., Brummer, G.-J., 2001. Cross-slope zonation of erosion and deposition in the Faeroe-Shetland Channel, North Atlantic Ocean. Deep-Sea Research I 48, 567–591.

Wunsch, C., 1975. Internal tides in the ocean. Review of Geophysics and Space Physics 13, 167–182.